Design, Simulation, and Construction of a Hot-Gas Bypass Chiller for a Commercial

Scale Psychrometric Coil Testing Facility

By

Khurram K. Makhani

Bachelor of Science in Mechanical Engineering.
Oklahoma State University
Stillwater, OK
2018

Design, Simulation, and Construction of a Hot-Gas Bypass Chiller for a Commercial

Scale Psychrometric Coil Testing Facility

Thesis Approved:

Dr. Christian K. Bach
_____
Thesis Advisor

Dr. He Bai
_____

Dr. Daniel E. Fisher
_____

ACKNOWLEDGMENTS

I am so grateful to have made it this far in my academic career. It would not have been possible without the support from all the people that helped throughout the years. I am blessed to be surrounded by such a strong support system. I would like to thank my family for always believing in me and pushing me towards excellence. Without their love and support, I would not have made it this far.

I would like to thank Dr. Bach for letting me join his research group back in 2017. I would not have even considered a Master's program if it were not for my participation in the lab during my undergrad. Dr. Bach has taught me so much through his lab and classes. With his guidance and thoughtful feedback, I have been able to improve my skills as an engineer. It is an honor to have such a great advisor.

I am so thankful for Aaron Bell and his dedication to my project. His help with brazing, wiring, and tubing is the reason I was able to complete the construction of the chiller. Working by his side, I gained a lot of useful knowledge that will last a lifetime. Additionally, I would like to thank Gary Thacker for his electrical expertise and for working with me on a tight schedule. I have learned a lot about electricity from Gary over the years and am eternally grateful.

I would like to thank all the members of BETSRG, past and present. The students within the group have helped and supported me since I joined back in 2017. A special thank you to Imran Chowdhury for working so well in coordination with me on our interconnect and dependent projects.

I would also like to give a special thank you to my girlfriend, Alex. She helped me so much this past year and I would not have finished this Master's program without her unconditional love and support.

Name: Khurram K. Makhani

Date of Degree: December, 2020

Title of Study: Design, Simulation, and Construction of a Hot-Gas Bypass Chiller for a Commercial Scale Psychrometric Coil Testing Facility

Major Field: Mechanical and Aerospace Engineering

Abstract: In recent years, there has been a large effort from industry and researchers to improve the efficiency of HVAC&R systems. At Oklahoma State University (OSU), the Building & Environmental Systems Research Group (BETSRG) has been developing a psychrometric coil testing facility to test commercial fin and tube heat exchangers. The facility has an array of subsystems; this thesis is focused primarily on the Hot Gas Bypass Chiller (HGBC) subsystem. The objective is to provide a source of cooling capacity for the pumped refrigerant loop and develop a controls strategy that will allow the chiller to adjust to quick changes in test points with minimal overshoot and settling time. To achieve the objective, a steady-state model was developed first for component sizing and parametric analysis. And second, development of a dynamic model to determine an optimal controls strategy for the HGBC and to establish a workflow on how to implement the controls strategy in the field.

TABLE OF CONTENTS

LIST OF TABLES

LIST OF FIGURES

ABBREVIATIONS

BETSRG	Building & Environmental Systems Research Group
EES	Engineering Equation Solver
EPC	Emerson Performance Calculator
EXV	Electronic Expansion Valve
GWP	Global Warming Potential
HGBC	Hot-Gas Bypass Chiller
MFG	Manufacturer
MIMO	Multiple Input Multiple Output
LQG	Linear Quadratic Gaussian
LQR	Linear Quadratic Regulator
OSU	Oklahoma State University
PID	Proportional Integral Derivative
PI	Proportional Integral
PRL	Pumped Refrigerant Loop
PV	Process Variable
SC	Subcool
SH	Superheat
SISO	Single Input Single Output
TEWI	Total Equivalent Warming Impact
VI	Virtual Instrument

NOMENCLATURE

VARIABLES	UNITS	DESCRIPTION
c_p	$\mathrm{J\,kg\,K}$	Specific heat
e	-	Control set point error
K_p	-	Proportional gain
K_i	-	Integral gain
K_d	-	Derivative gain
$\dot{m}_w$	kg/s	Mass flow rate of water
$\dot{Q}$	watt	Heat transfer rate
T_i	min	Integral time constant
$T_{w,exit}$	°C	Exiting water temperature
$T_{w,in}$	°C	Inlet water temperature
u	-	Control Process variable

CHAPTER 1

Introduction & Motivation

In recent years there has been a push from environmental conservation groups to reduce the environmental impact of HVAC&R systems. From 1990 to 2009 the emission of high Global Warming Potential (GWP) gases into Earth's atmosphere has more than tripled EIA (2011). To quantify the total impact of these emissions a value of Total Equivalent Warming Impact (TEWI) is used. TEWI is a measure of a refrigerant system's total environmental impact by including leakage, recovery losses, and energy consumption, as a function of GWP. Refrigerants such as R410A and R134a have GWPs in orders of magnitude above Carbon Dioxide. Therefore, when systems leak, their TEWI is increased by over 25% relative to the emissions caused by power production Bitzer (2014). With such a large impact on the environment, new low GWP refrigerants must replace high GWP Hydrofluorocarbons (HFCs). The performance of these new refrigerants must be tested in existing equipment and new technologies to ensure that their TEWI is lower than current HFCs. Oklahoma State University (OSU) is developing a unique facility to be able to test these new refrigerants. Kincheloe et al. (2021) developed and constructed a facility, referred to as a Psychrometric Coil Test Facility. The purpose of the facility is to provide researchers with the capability to test commercial size evaporative fin and tube heat exchangers.

1.1 Background

The Psychrometric Coil Test Facility is in its later stage of development and is planned to be completed by May 2021. The facility is split into two sections, the conditioning

side, and the test side. The conditioning side consists of the following components: humidifier, blowers, conditioning coils, and heating elements. The conditioning side will have effective airside control. On the test side, there will be a pumped refrigerant loop connected to the test coil. This refrigerant loop will carry the new low GWP refrigerants for testing. However, effective control of the refrigerant loop is still in development. For the refrigerant loop to be able to reject heat following the test section, it will require a dedicated chiller.

1.2　Project Objectives

This project focuses on the design, control development, and construction of the Hot Gas Bypass Chiller (HGBC). The objective is to provide a source of cooling capacity for the pumped refrigerant loop and develop a controls strategy that will allow the chiller to adjust to quick changes in test points with minimal overshoot and settling time. To achieve the objective, a steady-state model was developed first for component sizing and parametric analysis. Second, development of a dynamic model to determine an optimal controls strategy for the HGBC and to establish a workflow on how to implement the controls strategy in the field.

CHAPTER 2

Literature Review

2.1 Psychrometric Coil Testing Facility

The design and construction of the airside subsystem of the Psychrometric Coil Testing Facility was completed by Kincheloe et al. (2021). The design of the airside must be taken into consideration when developing the chiller. In addition, the placement of the chiller and pumped refrigerant loop is heavily dependent on the layout of the facility. The closed-loop airside subsystem contains both the test section of the facility and the conditioning section. Kincheloe's thesis also gave a detailed channel reference for the Psychrometric Coil Testing Facility Data Acquisition system. This was used to determine the input and output channels the HGBC can use.

Shown in Figure 2.1 is a schematic of the airside subsystem. The air flows across the test coil and is then guided by turning vanes to the conditioning section. The conditioning section adjusts the temperature, humidity, and flow rate of the air back to the coil inlet test condition. The air is guided back to the test coil completing the closed airside loop.
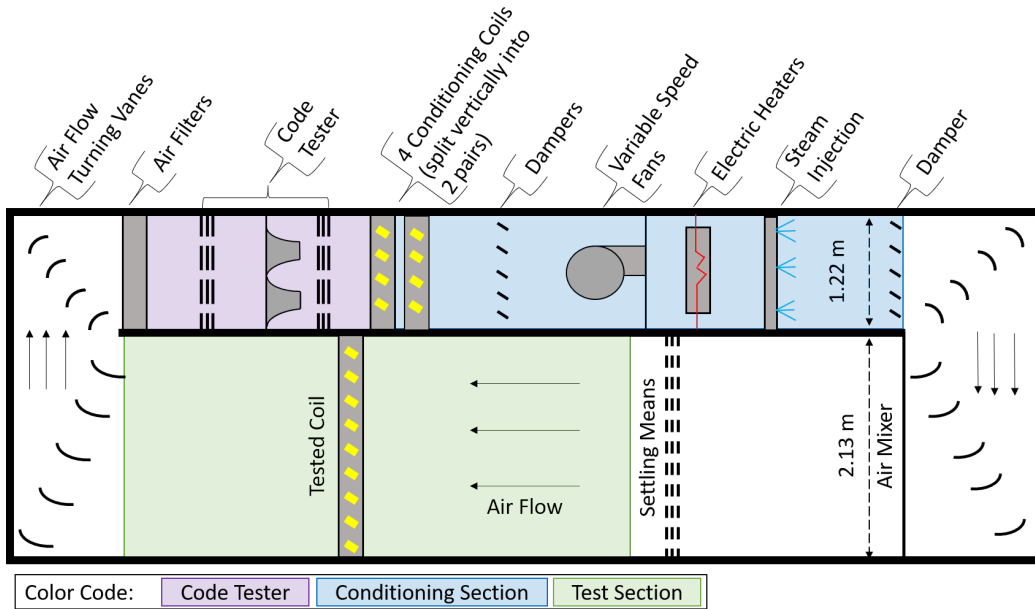
Figure 2.1: Airside Schematic - (Kincheloe et al., 2021)

2.2 Thermodynamic Model

To properly size components for the HGBC, a steady-state model must first be developed to represent the physical behavior of the system. Schmidt et al. (2019) developed a steady-state model for the Hot-Gas Bypass Compressor Load Stand at Oklahoma State University before selecting components. The software used was Engineering Equation Solver (EES) Klein and Alvardo (2020). The EES model was used to estimate system limitations and operating parameters. It is important to investigate a steady-state model because it will provide insight on how to size critical components such as heat exchangers, expansion valves, and tubing.

2.3 Dynamic Simulation

Different simulation environments such as MATLAB, Modelica, and GT-Suite were considered before developing a model. Tanveer and Bradshaw (2020) showed that after model initialization, Modelica was more computationally efficient (e.g., shorter computation time) than MATLAB and GT-Suite when using numerical differen-

tial equation solvers. Additionally, the acausality of Modelica makes models more reusable than traditional object-oriented programming languages (Fritzson, 2014).

Modelica offers a vast amount of third-party libraries, 30 of which listed on `https://www.modelica.org/libraries/ModelicaLibrariesOverview`, that allow the user to easily connect acausal models together. An example of this can be seen by Kaiser et al. (2018) in the development of a complex omnibus refrigeration cycle in Modelica, using the TIL Suite (2018) Library. The TIL Suite (2019) Library 'offers many robust models for vapor-liquid equilibrium (VLE) fluids in thermal components and systems. In addition, the TIL suite uses the geometry-based heat transfer and pressure drop correlations. The TIL Suite Library has many standard components for thermodynamic modeling such as compressors, heat exchangers, expansion devices, and separators. Therefore, it was determined to develop the HGBC dynamic model in Modelica. The integrated development environment (IDE) used was Dymola, provided by Dassault Systems. Dymola offers the entire model development process from model creation, simulation, and result analysis (Dassault Systèmes, 2019).

Winkler (2009) showed how the components of his model interacted with one another. Although Winkler did not use Modelica, his simulation model used many of the same principles that Modelica uses to solve the simulation. For example, the use of simultaneous evaluation of model equations. Winkler also gave tips on how to reduce simulation times, such as proper estimated initial values conditions and a limited number of segments for complex geometries such as heat exchangers. The trade off with a limited number of segments is accuracy versus computational time. The segment number should be enough to capture physical phenomena but not to the point where it negatively impacts simulation time.

2.4 System & Component Control Approaches

Many forms of control have been investigated for vapor compression cycles. The most prominent is the Proportional Integral Derivative (PID) feedback control. Marcinichen et al. (2008) claims that PI control is optimal for thermal systems because it is simple to implement, can minimize steady-state error, and can compensate for disturbances. Singleton et al. (2020) implemented a Single Input Single Output (SISO) PI feedback control to a hot-gas compressor load stand. Singleton explains how difficult it is to achieve steady-state for the load stand. The problem stems from SISO feedback control for the expansion valves and hot-gas bypass valves. The process variables are connected, therefore, when one variable changes, it causes a change in another. Once the PI controllers detect this change, they attempt to compensate for the deviation to the process variable. The PI controls begin to fight each other when the process variable reaches near the setpoint.

With the limitations of SISO feedback control, other options such as Multiple-Input Multiple-Output (MIMO) become more attractive. Jain and Alleyne (2009) show a MIMO control structure with a Linear Quadratic Gaussian (LQG) controller was able to achieve similar results compared to the SISO controller when applied to a vapor compression cycle. The difference between the controllers is when the setpoint changes across the operating range, the LQG controller has better setpoint tracking than the SISO controller. Furthermore, the LQG controller incorporates a cost function to relate all inputs to all outputs. This is beneficial because it allows the user to determine a weighted relationship between control variables and the process variables they are affecting.

2.5 Examples of Hot-Gas Bypass in Application

The HGBC is the source of cooling capacity for the pumped refrigerant loop. Therefore, the HGBC will need to make quick adjustments to capacity as the test points

change for the pumped refrigerant loop. According to global HVAC&R manufacturer Trane (2003), commercial chilled water systems that require instantaneous load changes will benefit from the incorporation of a hot-gas bypass valve. Benefits included quick neutralization of the refrigeration effect, continuous system operation, and sustains higher gas velocities which ensure adequate oil return to the compressor.

On-off cycling of the compressor is the method used in traditional HVAC&R systems. This method is easy to implement and works well when the setpoint temperature does not have a tight limit, such as the residential cooling applications. However, the downside is no precise control of capacity. Additionally, the cyclic behavior of the system causes wear and tear on the compressor. Therefore, with the incorporation of hot-gas bypass, refrigeration systems can operate continuously which reduces the cyclic fatigue on the compressor (Yaqub et al., 2000).

Experimental setups using hot-gas bypass in academia typically are compressor load stands. A 40-ton Hot-Gas Bypass Compressor Load Stand developed by Orosz et al. (2016) used a series of valves to control the suction pressure and superheat of the load stand. Additionally, Bradshaw (2014) summarized best practices of hot-gas bypass compressor load stand design and operation. There is no evaporator in compressor load stands. However, it is assumed that the thermodynamic design remains the same with an evaporator. Therefore, the best practices established from these setups were used as guidance for developing the HGBC.

CHAPTER 3

Steady State Thermodynamic Model & Component Selection

To fully understand the physical limitations of the HGBC in conjunction with a pumped refrigerant loop, a thermodynamic steady-state model was developed. Physical limitations such as minimum and maximum suction and discharge pressures are of interest when sizing components. In addition, important parameters such as mass flow rate and cooling capacity must also be considered when sizing. Simplifications and assumptions were made to be able to solve for all state points and additional parameters of the thermodynamic cycle.

3.1   Model Overview & Description

A multitude of software was used to achieve a reliable steady-state model for the HGBC. An EES (Klein and Alvardo, 2020) model was developed to solve for state points and parameters of the HGBC. The compressor performance map provided by Emerson-Copeland (2020b) was used to cross-validate the mass flow rates and isentropic efficiencies calculated in EES. Additionally, Hexact (Danfoss, 2018b), a heat exchanger sizing tool, was used to properly size braze plate heat exchangers and as another means to cross-validate the EES model. In relation to sizing, Hexact was the bridge between the HGBC and pumped refrigerant loop. This is because the HCBC provides the capacity to the pumped refrigerant loop via a refrigerant to refrigerant braze plate heat exchanger, otherwise referred to as a cascade condenser. Seen in Figure 3.1 is the preliminary piping and instrumentation diagram (P&ID) of the HGBC and the pumped refrigerant loop. The diagram illustrates the connections

between the test coil, pumped refrigerant loop, and the HGBC.
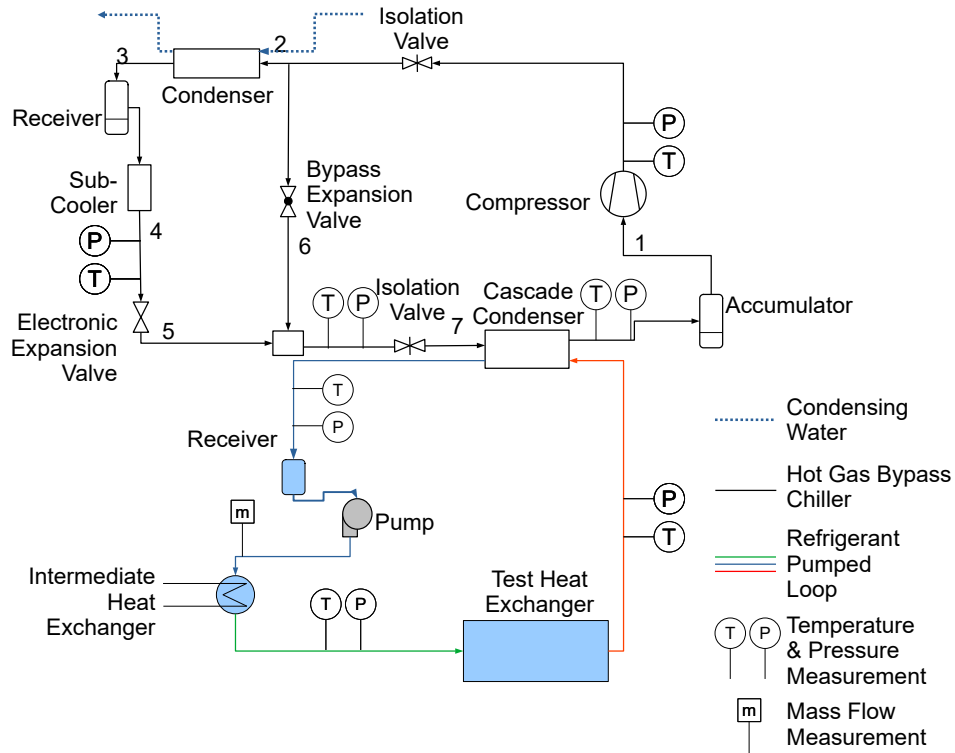
Figure 3.1: Preliminary HGBC & Pumped Refrigerant Loop P&ID

3.1.1 Design Constraints

The first major design constraint for the HGBC was the Psychrometric Coil Testing Facility's operating envelope. Kincheloe et al. (2021) specified that the facility can operate with a test coil air inlet temperature from 0°F to 140°F, with a maximum airflow rate of 8,000 CFM. In the commercial building setting, refrigerant-to-air systems typically are designed with an airflow rate proportional to the rated cooling capacity (e.g., 400 cfm/ton) (Cai and Braun, 2018). Therefore, the maximum cooling capacity that the HGBC should provide to the pumped refrigerant loop is 20 tons. The second design constraint is the pumped refrigerant loop. The loop must mimic the inlet and exit conditions an fin and tube evaporator will encounter in normal operating conditions. Table 1 of AHRI-Standard-540-2015 (2015) specifies the standard conditions

for commercial compressors, conditions such as suction dew point temperatures and return gas temperatures. The exit of the evaporator must match these suction/dew point temperatures to meet design requirements. With these required conditions in mind, the maximum design evaporating temperature of the HGBC is limited to -3 °C. Any higher evaporating temperature will cause the pumped refrigerant loop to operate outside of its specified design constraint, because return gas temperatures from the evaporator will be higher than design requirements. The final main design constraint is the condensing water inlet temperature. During the summer the lab chilled water can increase in temperature to around 18°C. Therefore, the worst case transient condition of 18°C was used in sizing the condenser.

3.1.2 Provided Components

Emerson Climate Technologies, Inc donated a Copeland ZPV0962E-7E9, a 20 ton (nominal) variable speed scroll compressor to OSU Building & Environmental Thermal Systems Research Group (BETSRG). There are many benefits to having a variable speed compressor such as precise control of capacity, increased Coefficient of Performance (COP) at part load, and oil boost. Oil boost means to ramp up compressor speed to increase oil return from low-speed operational conditions. Although, the HGBC will have precise control through the hot gas bypass, having another component that offers precision control will guarantee optimal control of capacity. Also, Danfoss donated a water control valve for flow control of the condensing water. The valve is rated for a maximum of 33 GPM.

3.1.3 Assumptions

The EES model requires making thermodynamic assumptions when calculating state point. These include constant compressor volumetric efficiency, a linear relationship between compressor curves for mass flow rate and isentropic efficiency, adiabatic

mixing, isobaric heat exchangers, and isenthalpic expansion valves. Furthermore, mass and energy balance equations within the model neglect kinetic and potential energy losses.

3.2   Overview of Employed Modelling Tools

To better understand the complex workflow of the steady-state model development, refer to Figure 3.2, which shows the coordination between multiple pieces of software. The reason for this type of workflow is due to the scope of work being split between the HGBC and the pumped refrigerant loop. Imran Chowdhury, a fellow graduate student at OSU, is responsible for the development of the pumped refrigerant loop. The results from both EES programs are used in Hexact to determine the appropriate heat exchanger. Once unknown heat exchanger parameters are calculated in Hexact, they are compared to the results from EES. If the parameter values in Hexact are not matching within 2% of the parameter values calculated in EES, the process is repeated by trying new input parameters within the EES models. Inputs such as superheat, subcooling, condensing temperature, and evaporating temperature are altered to match with the Hexact software.
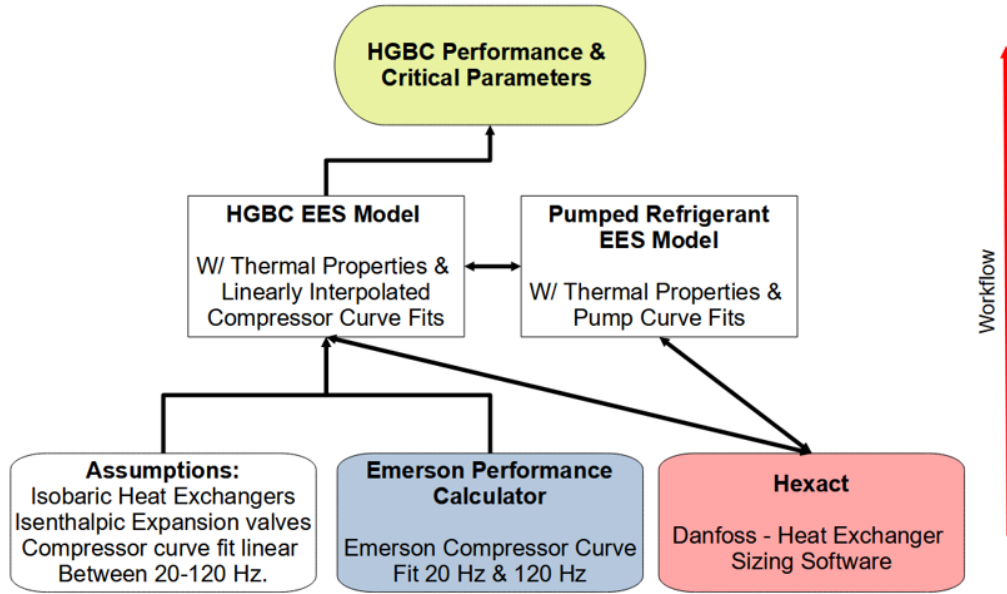
Figure 3.2: Steady State Model Workflow Chart

3.3 Modelling and Selection of Additional Components

The HGBC model in EES has a various amount of inputs and outputs. User-specified inputs include evaporating temperature, condensing temperature, subcooling, super-heat, compressor speed, and refrigerant type. The output of the model includes all main cycle state points and various critical parameters. Parameters such as mass flow rate, cooling capacity, and heat rejection. Additionally, the model outputs a Pressure versus Enthalpy (P-h) plot for the user to visualize the changes they make to cycle inputs. Figure 3.3 shows a P-h plot for the HGBC. The state point references match the state points in the P&ID seen in Figure 3.1. State point 7 is currently plotted with bypass ratio of 20%. As the bypass ratio increases the cooling capacity decreases. At 100% bypass ratio state point 7 will be equal to state point 1. The EES model does calculate the energy and mass balance between the hot-gas and the liquid line when mixing at state point 7 and will be discussed in detail in subsection 3.3.3.2
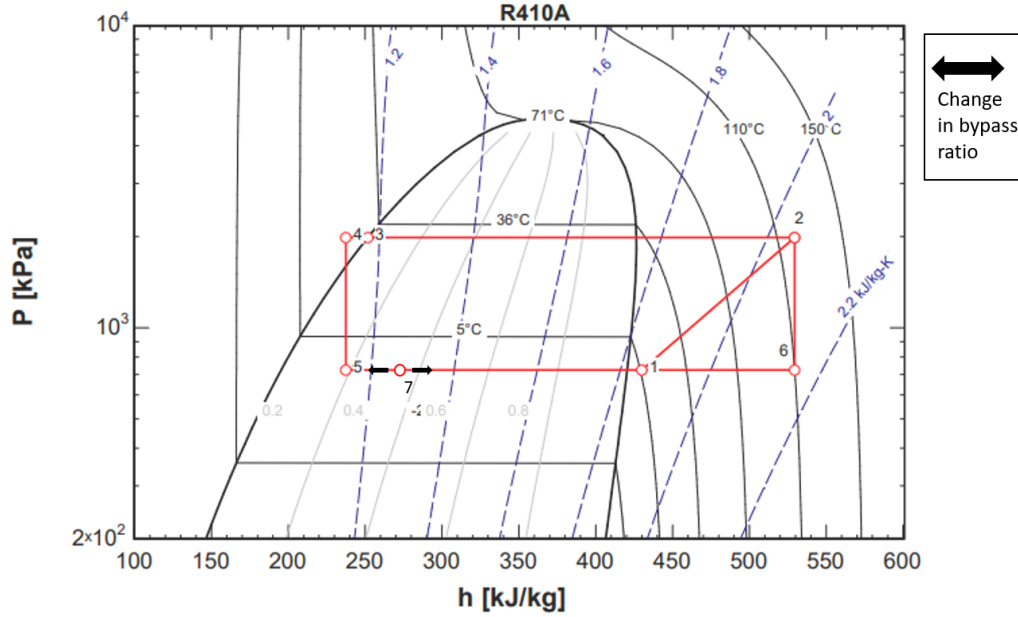
Figure 3.3: EES - Pressure vs Enthalpy Plot @ $n = 120Hz$, $T_{con} = 32°C$, $SH = 11.1K$, & $SC = 8.3K$

3.3.1 Compressor

To correctly map the mass flow rate, the EES model needs to account for the compressor's operating speed range. The ZPV0962E-7E9 is rated for 20 to 120 revolutions per second (Hz) at 3-phase 480 VAC. A ten-coefficient model was utilized to determine the mass flow rate at specific condensing and evaporating temperatures (AHRI-Standard-540-2015, 2015). The Emerson Performance Calculator (EPC) (Emerson-Copeland, 2020a) was used to determine the ten coefficients for 20 and 120 Hz. Then, the EES model used linear interpolation to determine the mass flow rate at any frequency based on the minimum and maximum speed of ten coefficient models. Equation 3.1 shows the linear interpolation method used in the model. Where n is the compressor speed in Hertz (Hz), $\dot{m}_{tot,20}$ and $\dot{m}_{tot,120}$ in (kg/s) are the mass flow rates from both coefficient models of 20 and 120 Hz, respectively.

$$\frac{\dot{m}_{tot,n} - \dot{m}_{tot,20}}{\dot{m}_{tot,120} - \dot{m}_{tot,20}} = \frac{n - 20}{120 - 20} \tag{3.1}$$

13
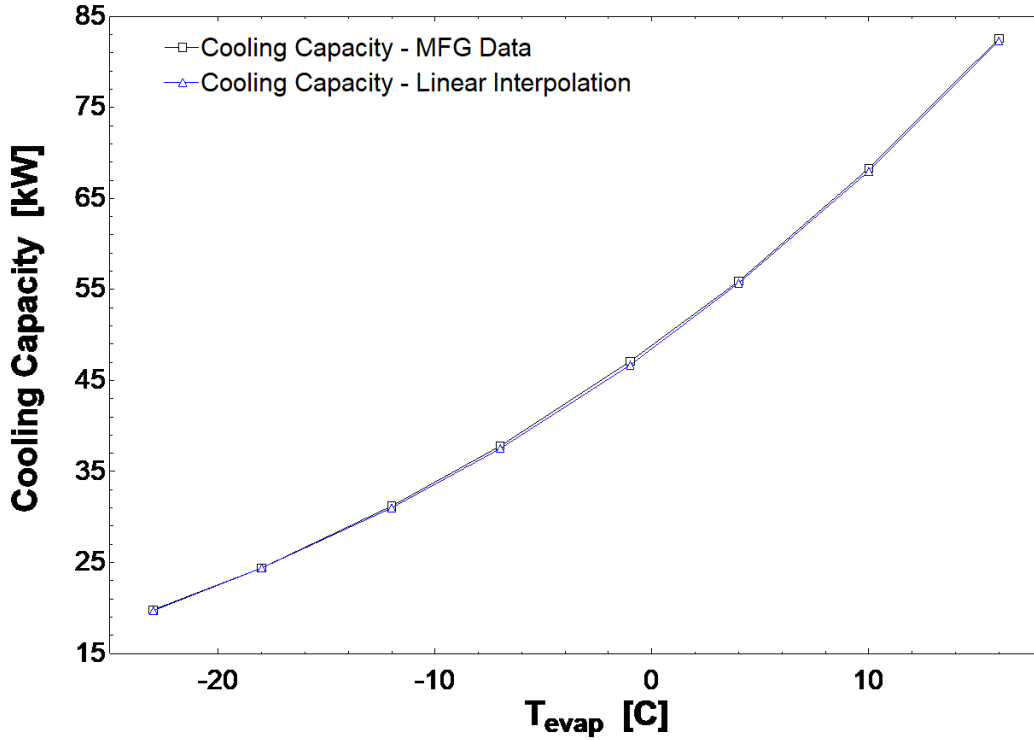
Figure 3.4: Cooling Capacity vs Evaporating Temperature @ $n = 90Hz$, $T_{con} = 32°C$, $SH = 11.1K$, & $SC = 8.3K$

The linear model was able to map the mass flow rate with a maximum error of 2.12% with respect to the compressor map provided by Emerson at 90 Hz. The maximum error occurred at the highest condensing and evaporation conditions at 90 Hz. Seen in Figure 3.4 is the cooling capacity vs evaporating temperature at 90 Hz operation. The manufacturing data taken from the compressor map was compared to the linear interpolated data calculated in EES.

Table 3.1: Condensing and Evaporating Temperature Envelope for 20-120 Hz Operation.

Temperature	MAX (°C)	MIN (°C)
Condensing	35	10
Evaporating	16	-29

To achieve the maximum range of compressor speed (20-120 Hz) the condensing and evaporation temperatures must be within the compressor operating envelope. Table 3.1 shows the minimum/maximum allowable evaporating and condensing tem-

14

peratures to achieve the full range of compressor speed. Additionally, Appendix F shows the full operating envelope of the ZPV0962E-7E9. With the compressor envelope in mind, the maximum design condensing temperature will be 32°C to ensure if the condensing temperature fluctuates at 120 Hz, it will not exceed the 35°C temperature limit.

The mapping of overall isentropic efficiency is similar to mapping the mass flow rate in relation to the linear interpolation for a range of frequencies. Although, the EPC did not directly output the ten-coefficient model for the overall isentropic efficiency, the EPC did output a ten-coefficient model for variable speed drive output power. The drive output power was treated as the electrical input power to the compressor. The electrical input power was linearly interpolated within EES the same as the mass flow rate shown above. Then, using the isentropic power calculated in EES the overall isentropic efficiency was determined. The overall isentropic efficiency is calculated as

$$\eta_{oi,comp} = \frac{\dot{W}_{isn}}{\dot{W}_{elc}} \tag{3.2}$$

Where $\dot{W}_{isn}$ is the isentropic power and $\dot{W}_{elc}$ is the electrical input power to the compressor, both in kilowatts (kW).

3.3.2 Heat Exchangers

Brazed plate heat exchangers were selected for all three heat exchangers because they are more compact in design than coaxial heat exchangers.

3.3.2.1 Condenser

To properly size the condenser, Danfoss provides a heat exchanger sizing calculator, Hexact (Danfoss, 2018b). The calculator requires inputs such as refrigerant mass flow rate, required load, inlet and outlet water temperatures, and more. The primary de-

sign constraint is the condensing water inlet temperature. Lab Chilled Water(LCW) will be used as the cooling water for this application. As seen in Equation 3.3 an energy balance is used to determine the temperature rise of the LCW. Where $(\dot{m}_r)$ and $(\dot{m}_w)$ are the mass flow rates of refrigerant and LCW, respectively. An LCW inlet temperature of 18°C was assumed to guarantee the chiller can operate even during hot days in the summer. The chiller's design condensing temperature will be 32°C to ensure that there is an adequate temperature difference to promote heat transfer to the LCW. To properly size the condenser, the maximum $(\dot{m}_r)$ must be taken into account. The maximum $(\dot{m}_r)$ of 0.3 kg/s occurs at 120 Hz with a condensing and evaporating temperature of 32°C and -3°C, respectively.

$$\dot{m}_r(h_1 - h_7) = \dot{m}_w c_p(T_{w,out} - T_{w,in}) \tag{3.3}$$

Using these inputs within EES, the energy balance gave a maximum LCW outlet temperature of 28°C. With all the parameters defined, the Hexact software output multiple heat exchangers that met the required parameters. The selection of the condenser was determined by the lowest surface margin and lowest pressure drop across the refrigerant side of the condenser. The surface margin is represented as a percent difference between the calculated required heat transfer surface area actual heat transfer surface area of the selected heat exchanger. A surface margin closest to 0% is selected to ensure the proper sizing of the condenser. C62L-C-80, an 80 plate, microplate heat exchanger was the selected condenser, with a positive margin of 6% and a pressure drop of 2.1 kPa across the refrigerant side. To validate the EES model the Hexact software outputs were cross-referenced. There is less than a 1% difference between the EES model and Hexact with respect to output parameters. Shown in Table 1 are the outputs from Hexact compared to EES.

Table 3.2: Cross Validation of Critical Output Parameters between EES and Hexact

Parameter	EES Output	Hexact Output
Refrigerant Mass Flow Rate	0.30 (kg/s)	0.30 (kg/s)
Refrigerant Outlet Temperature	32.0 (°C)	31.9 (°C)
Water Outlet Temperature	27.6 (°C)	27.5 (°C)

3.3.2.2 Subcooler

The purpose of the subcooler is to ensure only liquid enters the expansion valve. Otherwise, if the refrigerant liquid flashes it can cause a decrease in the refrigerant mass flow rate and system pressures (Kang et al., 2008). The decrease in system mass flow rate and pressures will cause the HGBC to fall out of steady-state conditions. Consequently, the pumped refrigerant loop will fall out of steady-state conditions. The deviation from steady-state could void experimental results. Therefore, to ensure only liquid enters the expansion valve the subcooler will decrease the high-pressure refrigerant's temperature to $8\ K$ below the saturation temperature. Balancing LCW between the subcooler and condenser was an iterative process that involved matching parameters between EES and Hexact. EES and Hexact converged with 2 GPM of LCW through the subcooler and 31 GPM through the condenser.

3.3.2.3 Evaporator

The primary purpose of the evaporator in the HGBC is to absorb heat from the pumped refrigerant loop. The evaporator will be an intermediate heat exchanger to the pumped refrigerant loop. The evaporator is downstream of the test coil, and exit temperatures from the test coil must match the conditions stated in Table 1 of AHRI-Standard-540-2015 (2015) to meet design requirements. Consequently, the evaporation temperatures of the HGBC side were determined based on conditions required by the pumped refrigerant loop. Using Hexact and both EES models, an iterative method was applied to determine the appropriate evaporation temperatures. Addi-

tional limitations to the evaporation temperature were due to the operating envelope of the compressor. It was determined that the maximum and minimum evaporating temperatures will be -3 °C and -23 °C, respectively. These evaporation temperatures were selected with the compressor operating envelope and pumped refrigerant loop design constraints in mind. Additionally, when iterating between the EES models and Hexact, it was determined to lower the HGBC superheat to 9 K. This change in superheat will ensure that the pumped refrigerant loop will be at desired discharge conditions leaving the cascade condenser. When sizing the appropriate evaporator, multiple variables were taken into consideration. One being to minimize pressure drop through the heat exchanger because pressure drop plays a role in reduced capacity. And two, to keep the channel velocity through the evaporator side high enough (e.g., 0.7-0.8 m/s) to ensure adequate oil return (Kennedy, 2019). The design was also based around R410A on both sides of the evaporator, but a parametric study was conducted to see how the evaporator will perform with different refrigerants on the pumped refrigerant side. Seen in Table 3.3 are the results of the parametric study conducted on the D118L-E-70, a 70 plate, microplate evaporator.

Table 3.3: Parametric Study of Different Refrigerants Across Evaporator (Condensing Side)

Parameter	R410A	R1234ZE	R134a	R407C
PRL Outlet Temperature (°C)	2.0	-1.2	-1.0	-1.7
PRL Dew Temperature (°C)	3.5	4.7	4.5	9.5
PRL Mass Flow Rate (kg/s)	.25	.27	.25	.24

3.3.3 Expansion Valves

The EES model assumes that both the Hot-Gas Bypass Valve (HGBV) and the liquid line expansion valve are isenthalpic and adiabatic. There are 2 primary forms of expansion valves used in refrigeration applications, thermostatic and electronic expansion valves. Thermostatic expansion valves are purely mechanical systems with no control from the user. On the other hand, electronic expansion valves can take

18

multiple inputs to adjust the position of the valve. For the HGBC both expansion valves will be electronic because the electronic valve type allows the user to specify the valve position. Additionally, electronic valves also allow implentation of custom controls such as SISO or MIMO controls specifically tuned for the system.

3.3.3.1 Liquid Expansion Valve

The purpose of the liquid expansion valve is to bring the refrigerant to suction pressure before the liquid refrigerant is mixed with the expanded hot gas from the bypass. Danfoss has a large variety of liquid electronic expansion valves (EXV). Danfoss provides a set of instructions on their data sheet to appropriately size the expansion valve (Danfoss, 2018a). Following these instructions, the ETS 12.5 was selected for the liquid EXV.

3.3.3.2 Hot-Gas Bypass Valve

The bypass valve expands the hot gas to suction pressure before it mixes with the liquid refrigerant. The mixing process brings the refrigerant to suction conditions. The following energy balance and mass balance were used to determine the mass flow rate required by the bypass valve to bring the refrigerant to suction conditions after mixing. Equation 3.4 is the energy balance for the hot gas bypass and liquid line, and Equation 3.5 is the mass balance between the two flows. Where $(\dot{m}_r)$ is the total refrigerant mass flow rate, $(\dot{m}_{by})$ is the bypass mass flow rate, $(\dot{m}_c)$ is the mass flow rate through the liquid line, and (ϵ) is the normalized bypass flow rate.

$$\dot{m}_{by}(h_6 - h_1) = \varepsilon \dot{m}_c(h_1 - h_5) \tag{3.4}$$

$$\dot{m}_r = \dot{m}_c + \dot{m}_{by} \tag{3.5}$$

As ϵ is varied from 0 to 1, the change in the capacity of the evaporator can be determined. When ε is equal to 1, the evaporator will have no load across it. The HGBC will have the capability to have no load across the evaporator, which needs to be considered when sizing the bypass valve. The size of the valve was determined from sizing tables provided on the Sporlan website (Sporlan, 2018). Sporlan requires that the discharge dew temperature is no lower than 27°C to ensure sufficient head pressure. This requirement acts as another design constraint for the HGBC. Using Sporlan's provided tables, the SDR-3 was selected as the hot-gas bypass valve for the HGBC (Sporlan, 2018).

3.4   HGBC Operating Range

Based on the design constraints and selected components the condensing temperature will remain fixed at 32°C. The minimum and maximum evaporating temperatures are -3°C and -23°C, respectively. Additionally, it is assumed that the compressor will operate at 120 Hz. Table 3.4 summarizes critical parameter limitations within the conditions stated above.

Table 3.4: Parameter Limitations @ $n = 120Hz$, $T_{con} = 32°C$, $SH = 9K$, & $SC = 8.3K$

Parameter	Minimum	Maximum
Evaporation Temperature (°C)	-23	-3
Suction Pressure (Bar)	3.6	7.3
Mass Flow Rate (kg/s)	0.14	0.30
Cooling Capacity (tons)	7.5	16

CHAPTER 4

Controls Development

4.1   Dynamic Model in Modelica

After the steady-state model and design were complete, the next step in developing the HGBC was to determine an optimal control strategy. However, a steady-state model cannot provide the capability to do control investigations because of the absence of transience. Therefore, a dynamic model must be developed in Dymola.

To build a model of the HGBC cycle in Dymola, the example cycle *AutomotiveAC-Cycle_R134a* from the TIL Suite (2019) Library was used as a starting point. Figure 4.1 shows the unedited version of the *AutomotiveACCycle_R134a*. The first step was focused on the replacement of components, specifically heat exchangers in the example cycle. The example cycle has VLEFluid to Gas Micro-Plate Extruded Tube (MPET) heat exchangers. To match the HGBC cycle, the MPET heat exchangers were replaced with plate heat exchangers. The condenser and subcooler were changed from VLEFluid to liquid Plate heat exchangers. The evaporator was changed to a VLFFluid to VLEFluid Plate heat exchanger. In addition, a temperature sensor at the outlet of the evaporator (condensing side) was replaced from a gas temperature sensor to a VLEFluid temperature sensor.

After the replacement of components, an investigation was conducted to determine which parameters, initial conditions, sub-models, and variables that need to be changed to match the physical dimensions and conditions of the HGBC. For example, the Plate heat exchangers have physical dimensions: pattern angle, wall thickness, pattern amplitude, and pattern wavelength. Unfortunately, these physical dimen-
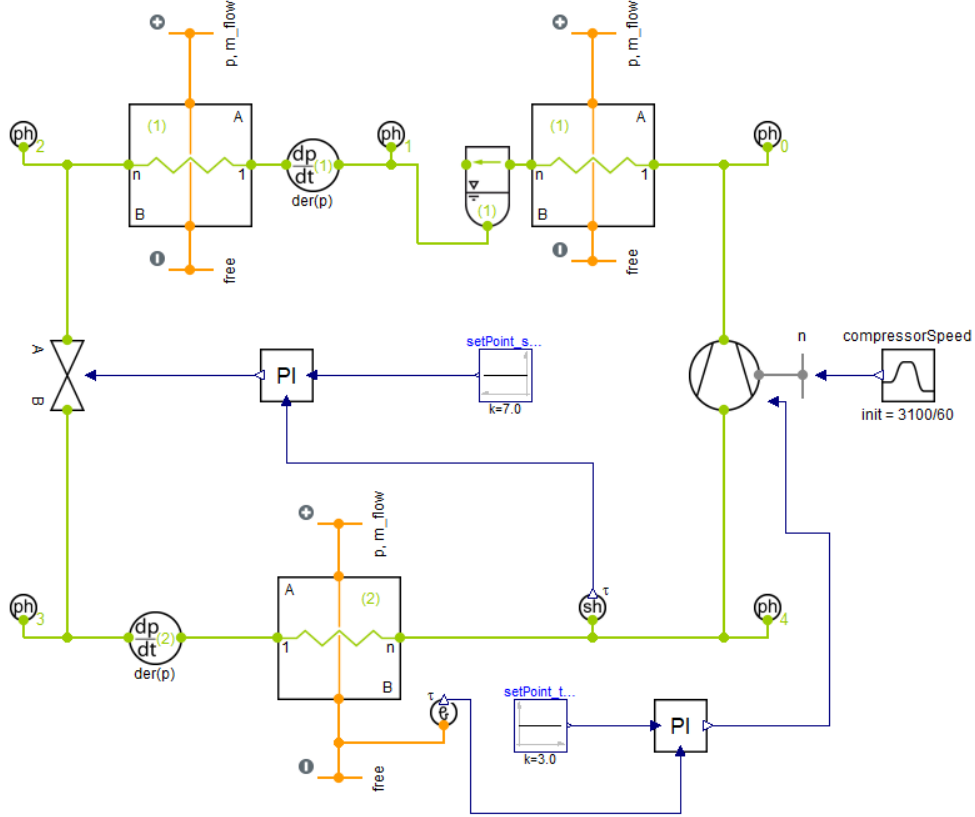
21

Figure 4.1: *AutomotiveACCycle_R134a*- TIL Suite (2019)

sions are proprietary information to the manufacturer of the plate heat exchangers. Therefore, the default values for pattern angle, wall thickness, pattern amplitude, and pattern wavelength from the TIL Suite (2019) were used. Figure 4.2 shows the HGBC model after components were replaced. Note, Figure 4.2 does not include the bypass valve or controls. The bypass valve was added after the steady-state solution in Dymola was cross-validated with the EES model's results at 0% bypass ratio. Furthermore, controls were incorporated after the bypass valve was added and results cross-validated with the EES model.

With new components in place, the next step was to change parameters within the sub-models to achieve the steady-state values seen in the EES model. A simulation of 1,000 seconds was set up to test the following changes in parameters. The simulation number of intervals was set to 1,000 (e.g. 1 interval/sec) and LSODAR was the solver
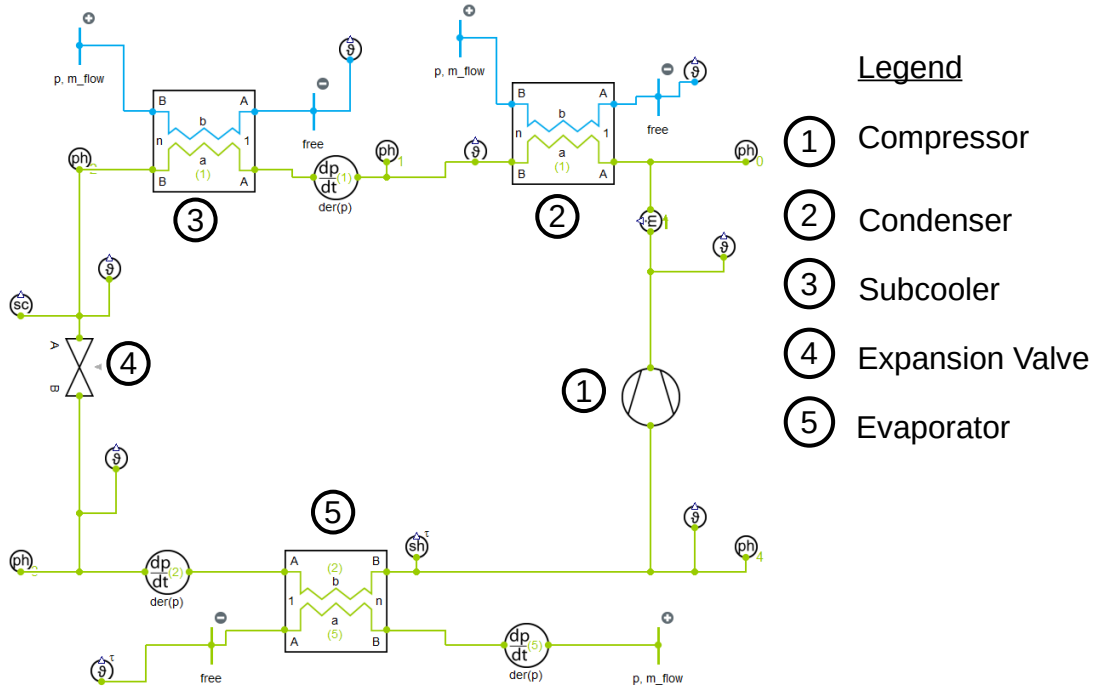
Figure 4.2: HGBC Model, No Bypass, Fixed Liquid Line Valve

used.

4.1.1 Heat Exchangers

The sizing of heat exchangers was first determined in EES. With the conditions specified and outputs from EES, the Hexact software provided by Danfoss was utilized in determining the appropriate physical size of the heat exchangers. The height, width, and the number of plates is part of the output from the Hexact software. These dimensions were used when specifying the heat exchanger geometry in Modelica. Additionally, boundary conditions for the condenser/subcooler liquid side and pump refrigerant loop were all specified. These boundary conditions can be seen in Table 4.1. Following the specification of heat exchanger geometries and boundary conditions, the next step was the determination of heat transfer and pressure drop correlations for the heat exchangers.

23

Table 4.1: Boundary Conditions for all Heat Exchangers

Boundary Condition	Condenser	Subcooler	Evaporator
Liquid $T_{w,in}$ (°C)	18	18	
VLEFluid T_{in} (°C)			18
$\dot{m}_w$ (kg/s)	1.87	0.13	
PRL $\dot{m}_{VLE}$ (kg/s)			.25

Since the EES model did not consider pressure drop through the heat exchangers, the Modelica model also ignored pressure drop. In respect to heat transfer models, The TIL Suite (2019) Library offers a variety of empirical correlations for determining the heat transfer coefficient. However, when attempting to utilize these correlations in the model, Dymola would either crash or output heat transfer coefficients that were unrealistically small. Therefore, the constant alpha correlation was utilized; alpha stands for a fixed heat transfer coefficient. The average heat transfer coefficients were provided as outputs from the Hexact software. Initially, the exact average heat transfer coefficients from the Hexact software were used in the Modelica model. However, the overall heat transfer still did not match the EES model. Consequently, the heat transfer coefficients were increased or decreased to match as best as possible to the EES model heat transfer values. Table 4.2 shows the Hexact heat transfer coefficients compared to the final heat transfer coefficients used in the Modelica model. Additionally, Table 4.2 shows the overall heat transfer of the Modelica model when the model reaches a steady-state compared to the EES model.

Table 4.2: Heat Transfer & Heat Transfer Coefficient Comparison @ $n = 120Hz$, $T_{con} = 32$°C, $T_{evap} = -3$°C, $SH = 9K$, & $SC = 8.3K$

HTC ($W/m^2 K$)	Hexact	Modelica	% Diff
h_{con}	1860	1860	0
h_{sc}	1650	1650	0
h_{evap}	930	1100	16.75
Heat Transfer (kW)	EES	Modelica	
Q_{con}	83.1	84.1	1.2
Q_{sc}	4.3	3.7	15
Q_{evap}	57.6	58.1	.86

4.1.2 Compressor

The EES model used a ten-coefficient regression model to map compressor mass flow and isentropic efficiency as a function of evaporating and condensing temperature AHRI-Standard-540-2015 (2015). Based on the ten-coefficient compressor model, at 120 Hz the compressor has an isentropic efficiency of 62%. When using 62% in the *EffCompressor* model from the TIL Suite (2019) Library, the compressor discharge temperature was 75 °C. The compressor discharge temperature in Modelica was 35% less than the EES model discharge temperature. Therefore, to match the EES compressor discharge temperature, the isentropic efficiency in the *EffCompressor* model was decreased to 32%. The isentropic efficiency is one of the only input parameters not matching the EES model.

4.1.3 Liquid Expansion Valve

For expansion valve modeling, the TIL Suite (2019) Library offers an orifice valve with an optional input for an effective flow area. An effective flow area for expansion valves is another proprietary piece of information for manufacturers. Therefore, a guess and check method was used to determine the effective flow area for the steady-state model case with a bypass ratio of 0%. The effective flow area was changed until the high-pressure and low-pressure side of the Modelica model matched those of the EES model within a 5% margin of error. The resulting effective flow area of for the liquid expansion valve was 5.57 μm^2. After the Modelica simulation reaches steady-state, the state properties are documented and compared with EES. Figure 4.3 shows a P-h plot comparison of the EES and Modelica Models with no bypass.

4.1.4 Hot-Gas Bypass Valve

After the steady state-model without bypass was validated with EES, the hot-gas bypass valve (HGBV) was added to the model. The orifice valve from the TIL Suite
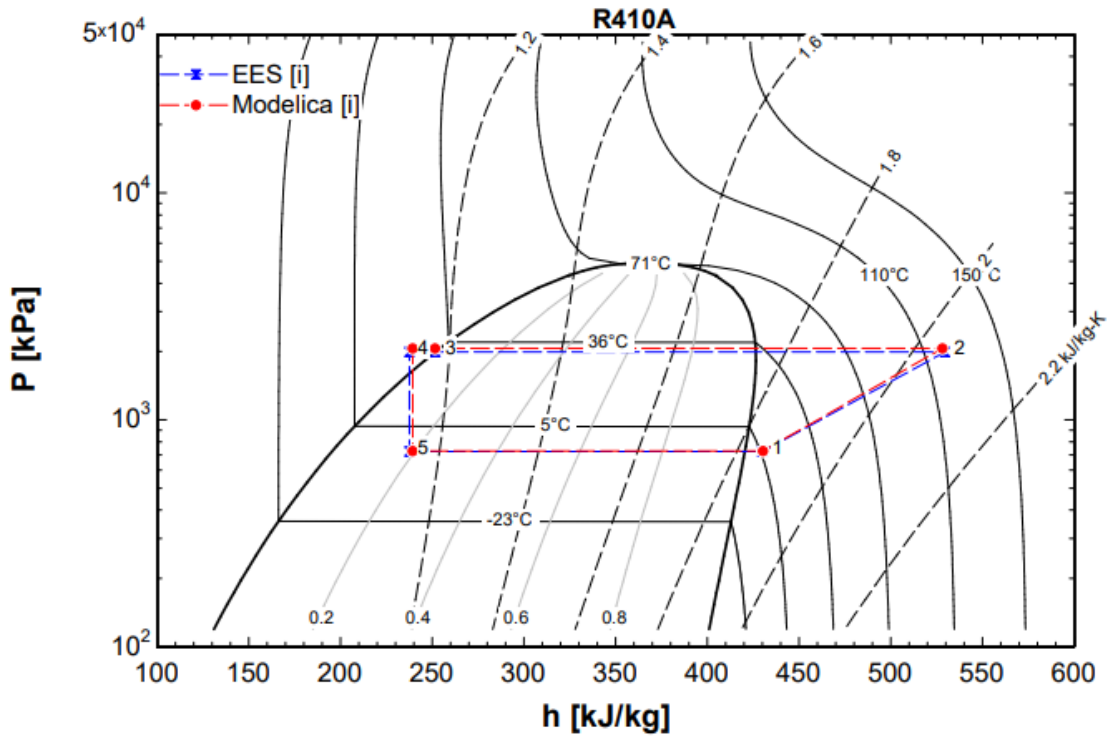
Figure 4.3: P-h Plot Comparison EES to Modelica, No Bypass, Fixed Liquid Line Valve

(2019) Library was used as the model for the HGBV. The same guess and check method was used to determine the effective flow area of the HGBV. A bypass ratio of 30% was selected to be the test condition for cross-validation between EES and Modelica. Table 4.3 shows the percent differences between the EES model and the Modelica model at 30% bypass. Note, the heat rejection from the condenser in the Modelica model is not matching the EES model, this is due to the mass flow through the condenser being higher in the Modelica model. The discrepancies between results are caused by the bypass valve. The EES model does not incorporate a change in suction pressure due to the bypass flow rate. The EES model assumes the isenthalpic bypass valve brings the superheated high-pressure refrigerant down to suction pressure. Additionally, the EES model assumes an isobaric mixing process. However, the total mass flow rate, subcooling, and superheat all match with the EES model. Therefore, it is determined that the model has successfully been cross-validated at

26

30% ratio with exception of heat rejection and mass flow ratios.

Table 4.3: Steady State Comparison @ 30% Bypass

Parameter	EES	Modelica	% Diff
$\dot{m}_{con}$ (kg/s)	0.19	0.22	14.6
$\dot{m}_{bypass}$ (kg/s)	0.11	0.08	31.5
T_{SC} (K)	8.3	8.1	2.50
T_{SH} (K)	9.0	9.4	4.35
Q_{con} (kW)	52.6	63.5	18.8
Q_{sc} (kW)	2.7	2.4	11.8
Q_{evap} (kW)	36.4	36.5	0.27

4.1.5 Superheat Controller

Once the Modelica model with a 30% bypass ratio was cross-validated with EES, the control loops were added to the Modelica model. To control the outlet superheat from the evaporator, a PI controller was added to the model. The change in superheat is due to inlet conditions at the evaporator. Inlet evaporator conditions are affected by the expansion valve effective flow area and bypass ratio. Therefore, the PI controller output signal is the effective flow area for the expansion valve. The process variable is the evaporator superheat and the setpoint is a constant input signal.

The control structure for the superheat PI controller is

$$u(t) = K_p[e(t) + \frac{1}{T_i} \int_0^t e(t)dt] \tag{4.1}$$

With $u(t)$ being the output signal with units (m^2), $e(t)$ is the error between the setpoint and process variable, (K_p) is the proportional gain, and (T_i) is the controller time constant.

Tuning rules were applied to properly tune the controller for minimum overshoot and settling time. The Ziegler and Nichols (1985) tuning method was the approach used for the superheat controller. The 30% bypass ratio condition was used as the test condition for comparison before and after tuning. The simulation starts with the

initial value for the effective flow area of the expansion valve, then the controller is activated at (t = 400 sec) with a setpoint of 9 K. The superheat response to the setpoint change is analyzed for controller effectiveness. Figure 4.4 shows superheat as a function of time before tuning rules were applied and Figure 4.5 shows the same plot but with tuning rules applied. The steady-state error was compensated for with the tuning rules.
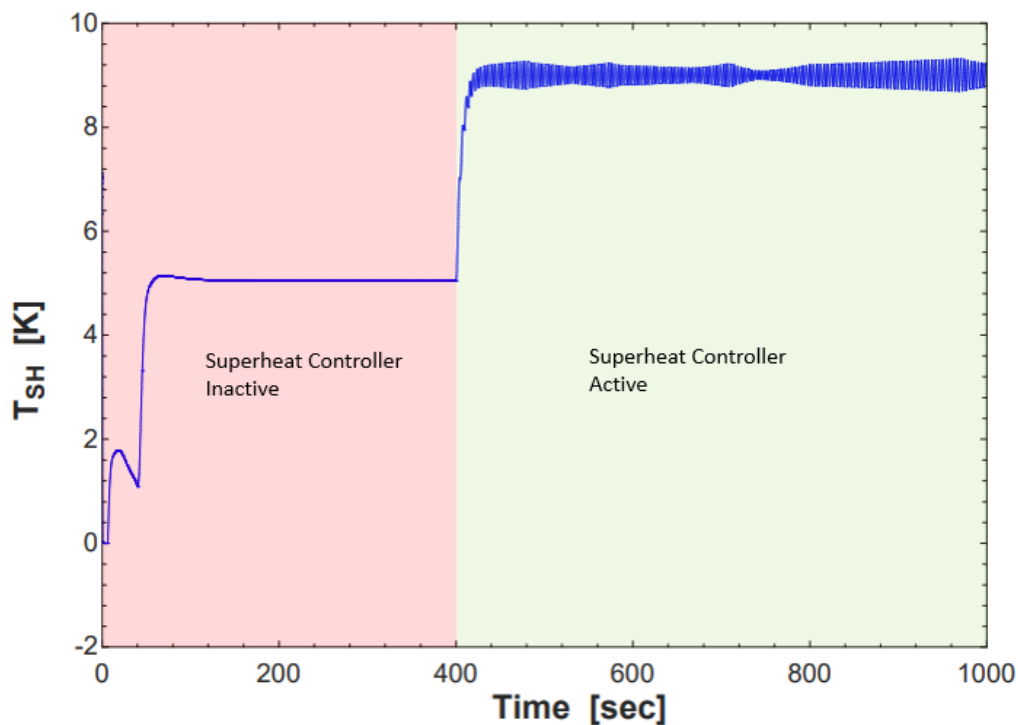

Figure 4.4: Superheat vs.Time Before Tuning, @ 30% Bypass

4.1.6 Bypass Valve Controller

The outlet pressure of the evaporator is affected by the bypass flow rate. The higher the bypass flow rate, the higher the outlet evaporator pressure. It was determined to add a second PI controller to the Modelica model, to control outlet evaporator pressure. The output signal of the PI controller is an effective flow area to the HGBV. The process variable for the controller is the evaporator outlet pressure. The same
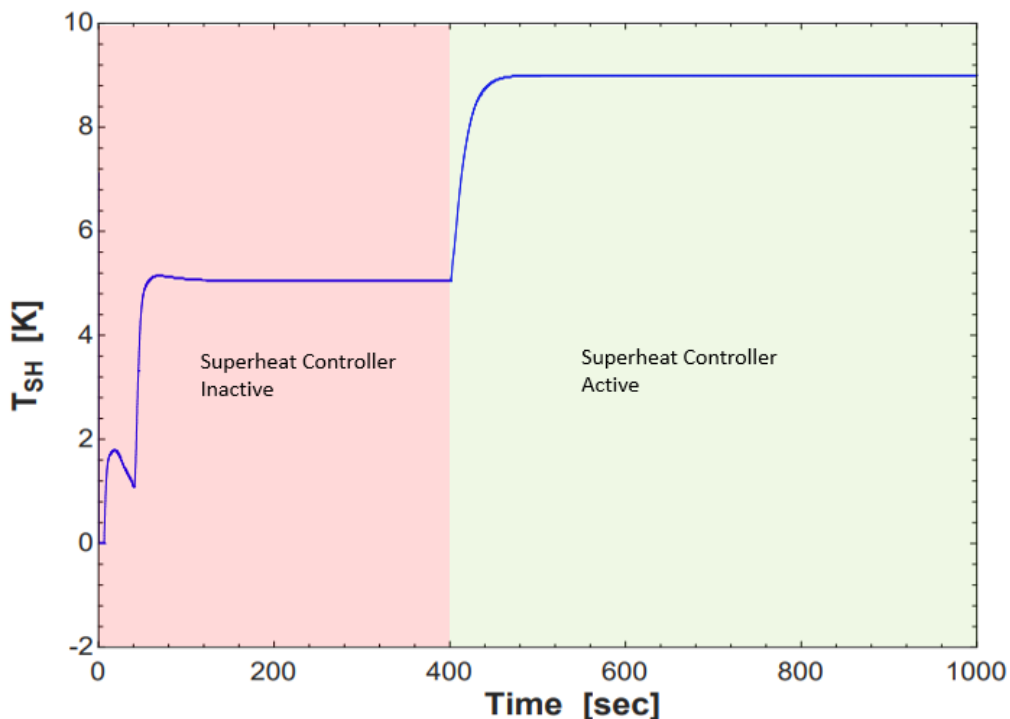
Figure 4.5: Superheat vs. Time After Tuning, @ 30% Bypass

PI control structure shown in Equation 4.1 was used for the bypass valve controller. Additionally, the Ziegler and Nichols (1985) tuning method was also applied to the bypass valve controller. The same test method for controller performance was also applied by delaying the controller start time to (t = 400 sec). Figure 4.6 shows the suction pressure as a function of time, with tuning rules applied to the bypass valve controller at 30% bypass. The suction pressure reaches the setpoint with no overshoot.

The simulation results did raise concerns about the effect of two separate PI controls. The superheat controller activates at (t = 0 sec) and once the bypass valve activates at (t = 400 sec), the superheat deviates from the setpoint. Figure 4.7 shows the superheat to drop to 0 K (e.g. two-phase vapor). If two-phase vapor enters the compressor in the application, it can cause damage to the scroll compressor. However, the superheat controller was able to eventually compensate for the deviation.
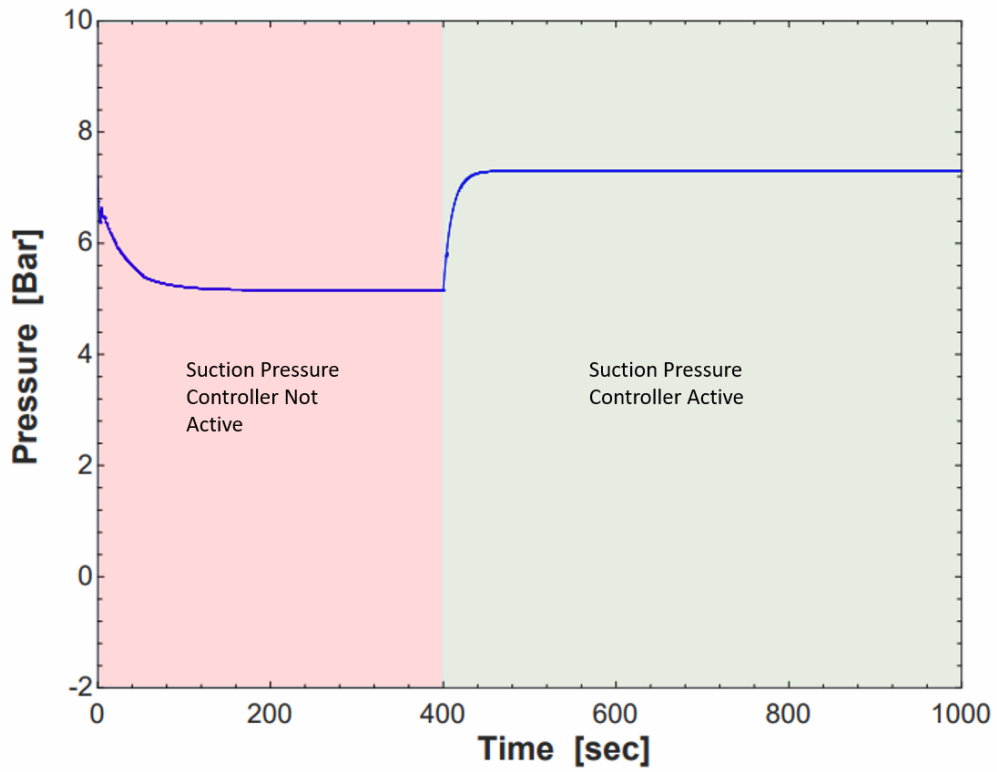
29

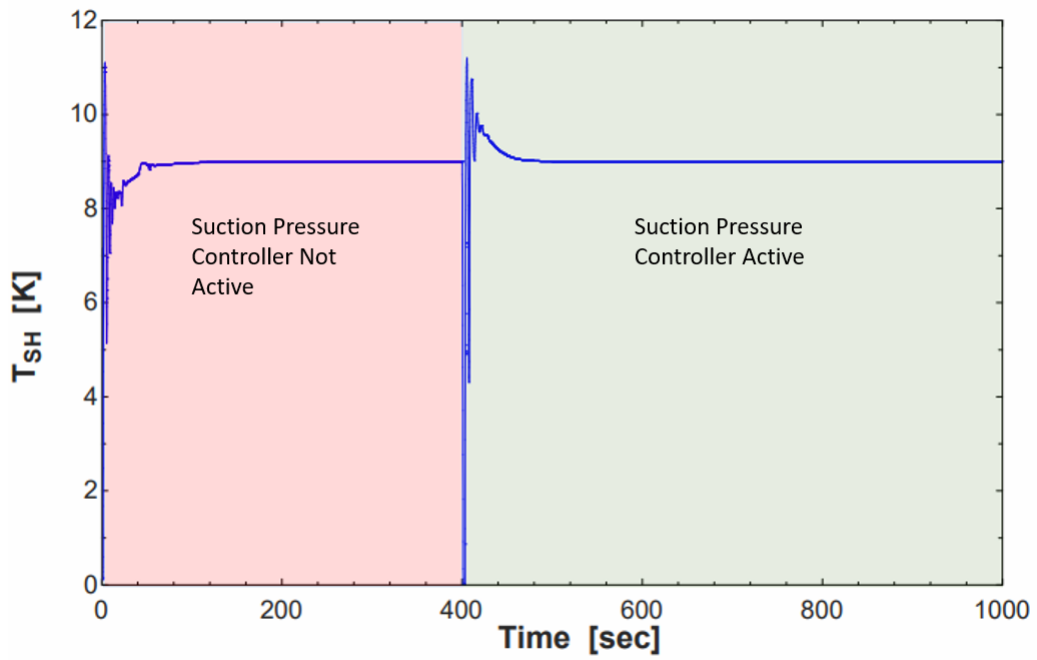Figure 4.6: Suction Pressure vs.Time After Tuning, @ 30% Bypass

Figure 4.7: Superheat vs.Time, 2 PI Controllers, @ 30% Bypass

Additional testing was conducted with both PI controllers by simulating the Modelica model at 100% bypass. Furthermore, step changes to the compressor speed were used as a means of external disturbance for the Modelica model. The change in operating conditions caused the PI controllers to fight each other when they were near their setpoints. However, the compressor speed disturbance does not seem to be reflected in the superheat and suction pressure. Therefore, further investigation will be needed on why the compressor speed does not cause fluctuations in the superheat and suction pressure. Figure 4.8 shows the superheat, suction pressure, and compressor speed versus time. With the PI controllers being SISO, they cannot compensate for another. The PI controllers have no information on the other controller's response behavior or the effect on the process variable. Consequently, the need for investigating a form of MIMO control becomes necessary for the HGBC.
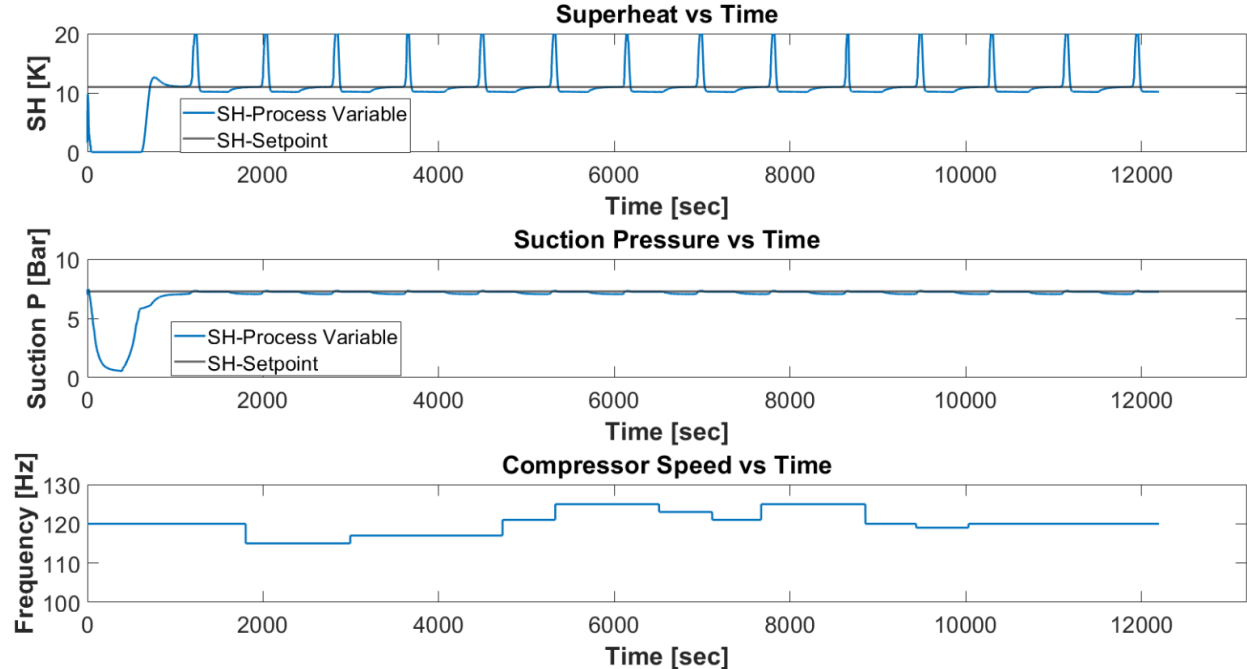

Figure 4.8: Superheat & Suction Pressure vs.Time, 2 PI Controllers, @ 100% Bypass (i.e. no load across evaporator)

4.2   MIMO Control

When investigating MIMO controllers in relation to thermal systems, there were two major types of controllers that stood out in relation to disturbance rejection and the cross-coupling of inputs to outputs. The H_∞ controller approaches the control problem as a mathematical optimization problem, and solves the optimization by analyzing the *Hardy Space* of matrix-valued functions of the system. The downside to the H_∞ controller is the level of mathematical knowledge needed to create such a controller (Rahman et al., 2017). The second MIMO controller type that was investigated was the Linear Quadratic Gaussian (LQG) controller. The LQG controller is a combination of the Linear Quadratic Regulator (LQR) controller and the Kalman Filter (Rahman et al., 2017). The advantage of the LQG controller is the incorporation of the Kalman Filter, allowing the controller can account for linear uncertainty and white noise. However, the Modelica model does not simulate white noise. Therefore, it was determined to use the LQR control design for the Modelica model. The LQR control implementation in Modelica will establish a workflow that can be applied to the actual HGBC. The only difference in application will be to apply the LQG controller to account for noise and uncertainty, but the established workflow from simulated data will remain the same.

With simulated data being discrete, the discrete LQR controller was chosen. The discrete LQR controller uses the state-feedback law shown in Equation 4.2. The state-feedback is input into a quadratic cost function shown in Equation 4.3. The matrices Q and R are user-defined weighted relationships between states and control inputs, respectively MATLAB (2020). This is one downside of the LQR controller in that it requires the user to have an understanding of the relationship between inputs and outputs.

$$u = -Kx[n] \tag{4.2}$$

$$J = \sum_{n=0}^{\infty} [x^T Q x + u^T R u + 2x^T N u] \tag{4.3}$$

4.3   System Identification

To apply the LQR controller in Modelica a state-space model is necessary. Following the example given by Jain and Alleyne (2009) the System Identification (ID) method was used to determine relationships between inputs and outputs. Input and output data were collected from the Modelica model and then imported into MATLAB. The System Identification Toolbox in MATLAB offers a function (*ssest*) that takes input and output data and determines a linear relationship with a state-space model. The form of the state-space model is shown in Equation 4.4 MATLAB (2020).

$$x[n + 1] = Ax[n] + Bu[n]$$
$$y[n] = Cx[n] + Du[n] \tag{4.4}$$

The capacity across the evaporator is heavily dependent on the suction pressure and superheat. Therefore, the suction pressure and superheat were the two outputs selected for System ID. The inputs relating to the suction pressure and superheat are the expansion valve effective flow area and the bypass valve effective flow area, respectively. Another version of the Modelica model was created with the same acausal models. However, instead of having PI controllers outputting the effective flow area to the valves, the *stepInput* block was used. A random Gaussian sequence for both effective flow areas was used as inputs to the valves. The open-loop Model results are shown in Figure 4.9.

The outputs of suction pressure and superheat were recorded along with the inputs in an Excel file. The Excel file was then read into MATLAB and the data was converted into a *iddata* object. The *iddata* object is the input to the (*ssest*) function.
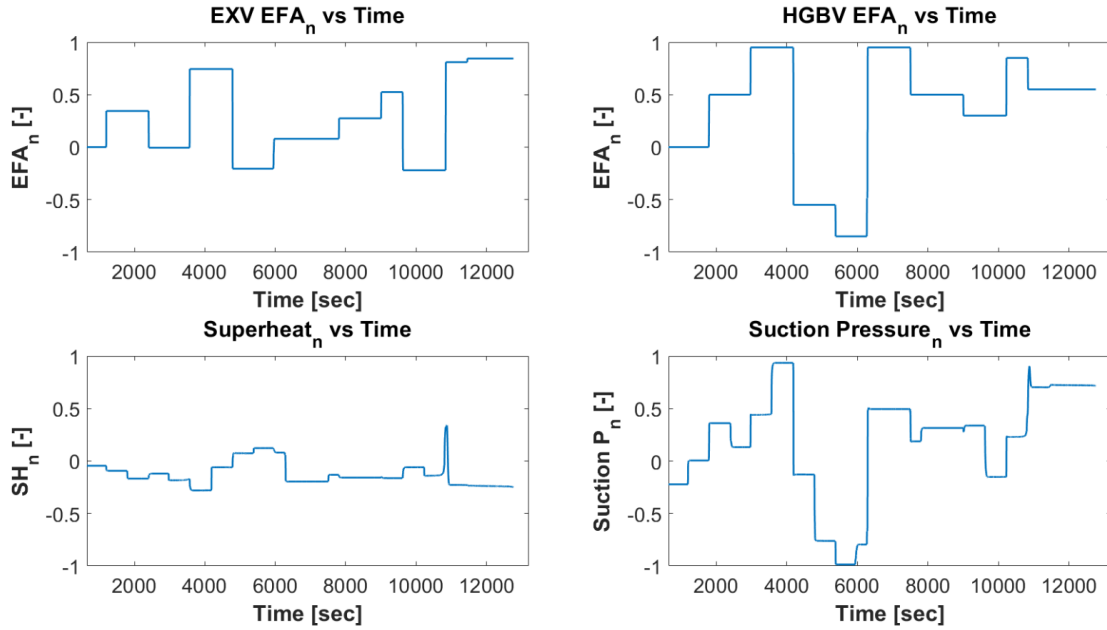
Figure 4.9: Open Loop I/O Results, Modelica Model @ 100% Bypass

The (*ssest*) function can either provide a best fit state-space model or the user can specify the order of the system. It is assumed that the model of the HGBC is a 2nd order system. Only the first half of the data set is used for System ID. The second half of the data is used to compare the created state-space model to the output data. The comparison is done by taking the second half of the data set inputs and entering them into the state-space model. The outputs from the state-space model are then compared to the actual outputs from the data set. Shown in Figure 4.10 is the comparison plot generated in MATLAB.

The percentages displayed in Figure 4.10 are the normalized root mean square error (NRMSE) of the Goodness of Fit (GOF) between the state-space model and simulated data (MATLAB, 2020). At first, the suction pressure GOF was above 70%. However, concurrently the superheat GOF was below 40%. To resolve this issue the inputs and outputs were normalized around their nominal operating condition. This allowed the inputs and outputs to be within the same order of magnitude. With normalized inputs and outputs, the GOF of both suction pressure and superheat were above 50%. The reduced order model is limited because it only considers two
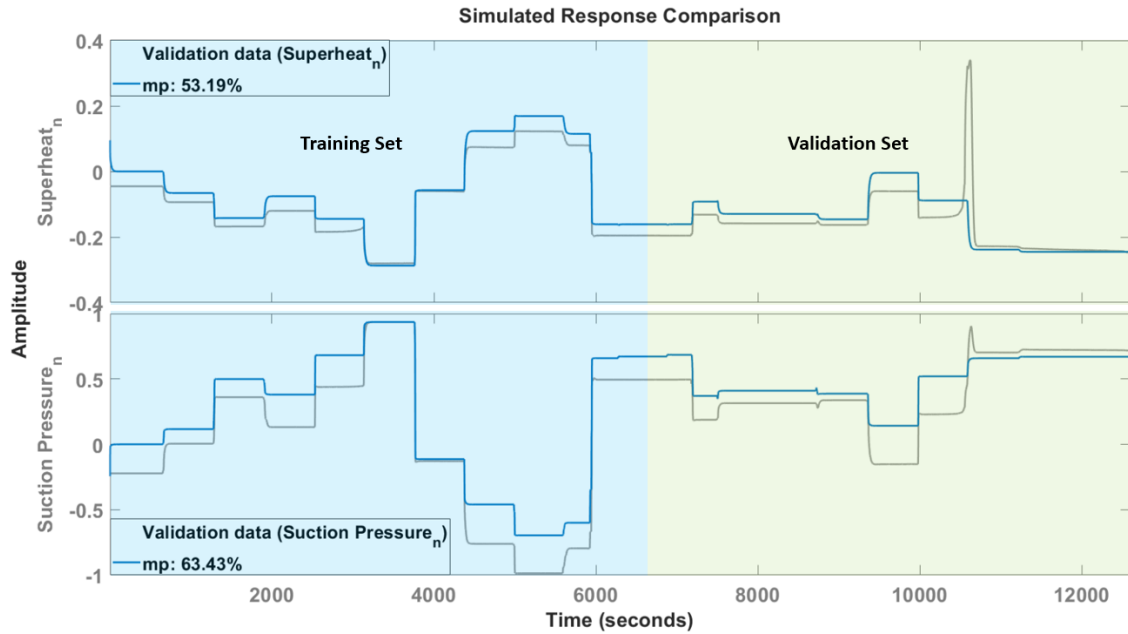
34

Figure 4.10: Comparison Results Between State-Space Model and Simulated Data, Modelica Model @ 100% Bypass

states, superheat and suction pressure. To achieve a more robust state space model, more states must be taken into consideration. However, the goal of developing a workflow for experimental data is still satisfied because the process will remain the same for System ID.

4.4   LQR Controller

MATLAB provides a discrete LQR function ($dlqr$) that has inputs of the state-space model, Q and R matrices, and the disturbance input. The state-space model with a GOF over 50% for both suction pressure and superheat was selected for controller development. Q is the weighted relationship of states, therefore, it was determined that Q will be the full state matrix of the system. Seen in Equation 4.5 shows how the Q matrix was determined. The R matrix was left as an identity matrix and can be changed after a relationship is determined on the weighted relationships of control input effects to the process variables.

35

$$I = \begin{bmatrix} 1 & 0 \\ 0 & 1 \end{bmatrix}$$

$$Q = C^T I C$$

(4.5)

After cost function analysis, the $(dlqr)$ function outputs the gain matrix K for the LQR controller. With a gain matrix for the LQR controller selected, a controller block was created in Modelica. Shown in Figure 4.11 is the Signal-flow graph of the implemented MIMO controller in Modelica. To mitigate steady-state error, an integral feedback control loop is added.
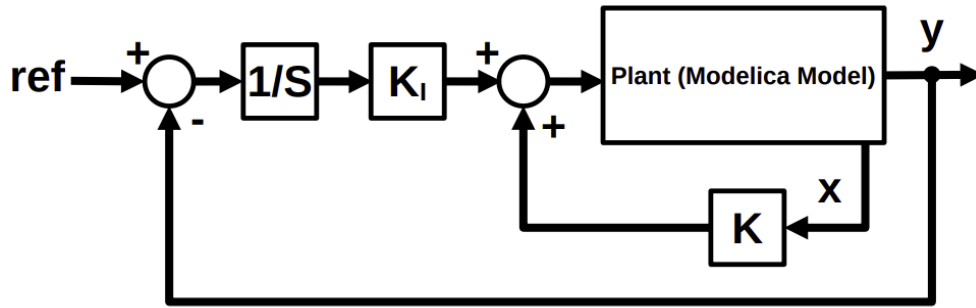

Figure 4.11: Signal-flow Graph of MIMO Controller for HGBC in Modelica

The proportional gain matrix K is multiplied by the states of the system – superheat and suction pressure. To accomplish this controller in Modelica a MIMO block was created for the LQR calculations. The created MIMO block extends from the base Modelica MIMO block. Inputs to the block are the superheat and suction pressure which are then converted to their full states. The gains solved for in MATLAB are then matrix multiplied to the full state matrix giving the output control signal. The output control signal is the effective flow area and is summed with the integral feedback control signal. The integral feedback loops were modeled using the PI control block from the TIL Suite (2019) Library. However, the proportional gain of the PI block was set to zero. The outputs from the MIMO block and PI blocks

were summed together and sent as inputs for the effective flow area of the expansion and bypass valves. The structured text for the MIMO block and the diagram window of the MIMO Modelica model can be seen in Appendix D.

4.5 MIMO Control Results

With the LQR controller successfully implemented in Modelica, a test was conducted to determine controller effectiveness in relation to settling time and mitigation of steady state error. The benchmark to compare to was the PI controller test condition seen in Figure 4.8. The LQR controller results are seen in Figure 4.12. Note, the superheat had less steady-state error than the PI controller benchmark. However, the suction pressure had larger steady-state error than the PI controller. Therefore, a parametric study must be conducted on the effects of control inputs on process variables.
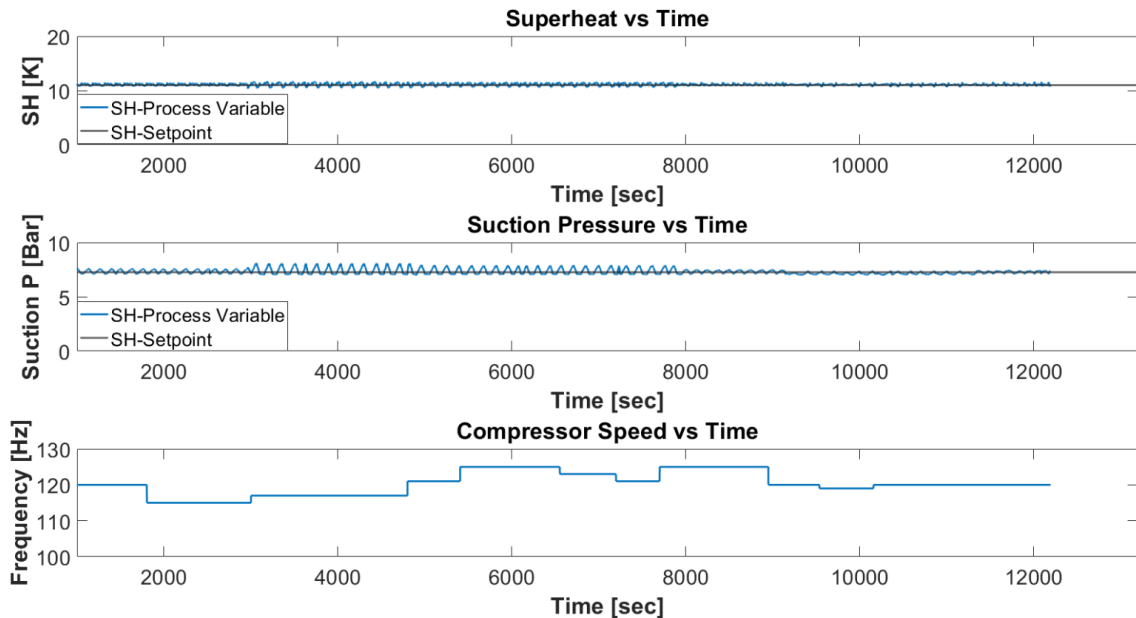

Figure 4.12: Superheat & Suction Pressure vs.Time, MIMO Control, @ 100% Bypass

Root Mean Square Error (RMSE) is the unit of measure used to compare the effectiveness of the SISO PI controllers versus the MIMO LQR controller. Shown in Table 4.4 the RMSE between the process variable and the setpoint for both control

structures. The MIMO controller shows an almost one order of magnitude reduction in superheat error. However, it lead to a more than 60% increase in suction pressure fluctuations. The main reason for this is suspected to be a limited GOF of the MATLAB model. Future work should include utilizing a Functional Mock-Up Unit (FMU) (Blochwitz et al., 2019) that uses the Modelica code directly. However, the developed current process is directly applicable for the physical setup and can therefore be applied with minimal changes. This workflow can be implemented with actual data once the HGBC construction phase is complete.

Table 4.4: RMSE Comparison Between Control Structures @ $T_{con} = 32°C$, $SH = 11K$, & $SC = 8.3K$

RMSE	SISO PI Controller	MIMO LQR Controllor
Superheat (K)	2.2	.23
Suction Pressure (Bar)	.16	.26

CHAPTER 5

Conclusion and Future Work

5.1   Conclusion

System components were properly sized and selected with a steady-state model developed in EES. A dynamic model was developed with Modelica to investigate different control strategies. Additionally, a MATLAB workflow was established for a MIMO controller for the HGBC. Although the MIMO control structure was applied with simulated data, the controls development workflow will remain the same with experimental data, other than minor rescaling of variables. However, the addition of the Kalman Filter will be the only difference when applying the MIMO control structure to the physical HGBC. Construction of the HGBC is complete in relation to piping, tubing, sensors, safety circuit, valve controls, and LabVIEW. The programming of the compressor variable frequency drive (VFD) is all that remains before the HGBC can be tested. However, the objective of experimental validation of the different control strategies will not be accomplished due to time constraints.

5.2   Current Status of Construction

To assist with the large scope of the project, it was decided to make the construction of the HGBC a Senior Design Project at OSU. The scope of the Senior Design team was to build the HGBC with industry standard compliance, develop a LabVIEW program for HGBC that works with the existing Psychrometric Coil Testing Facility LabView program, and to develop a Standard Operating Procedure (SOP) (Richey et al., 2020). However, due to outbreak of a global pandemic the Senior Design Project

scope was limited to a Solid Works model, LabVIEW code, and SOP development. Figure 5.1 shows the progress the Senior Design team made on construction of the HGBC versus the current status of construction. The Senior Design team's P&ID along with a detailed Solid Works model was used to continue construction when the University reopened. With the assistance of Advanced Technological Research Center (ATRC) personnel, the construction of the HGBC chiller was completed November 2020. Currently, controls and instrumentation wiring are being terminated. The goal is to test the HGBC with the LabView Virtual Environment (VI) developed by the Senior Design team. The LabView code currently is designed to incorporate PID control. The PID control will be the benchmark for controls testing of the HGBC. To achieve a LQG controller in LabView, the user must combine the LQR VI and Kalman Filter VI National Instruments (2009).
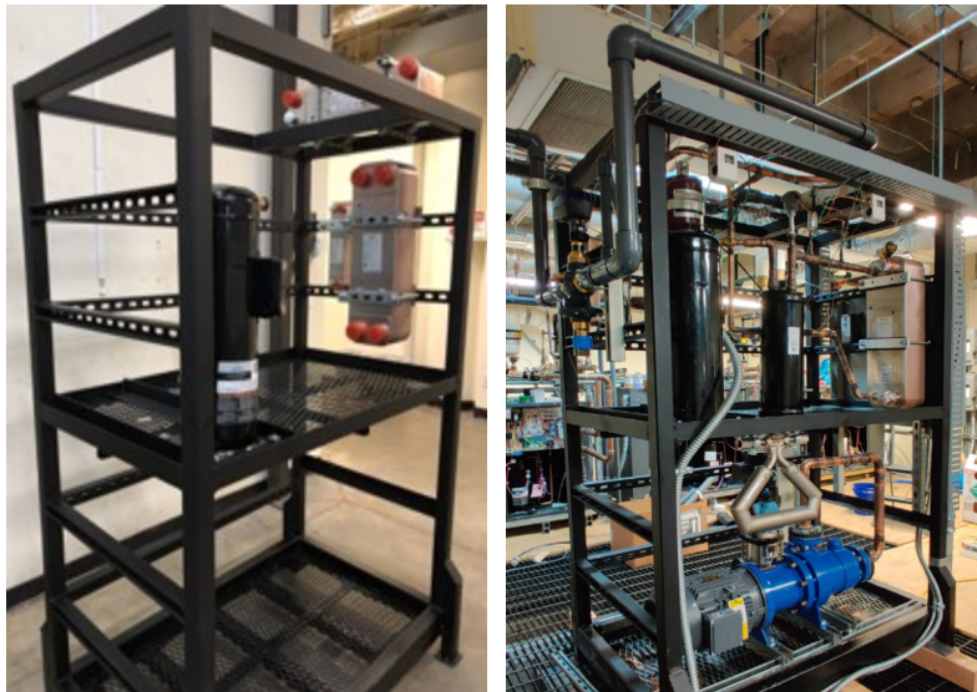

Figure 5.1: Senior Design Stopping Point (left), Current Status of Construction as of 11/16/2020 (right)

5.3 Simulation Improvements

Multiple steps can be taken to increase the fidelity of the Modelica model. For example, the incorporation of RefProp (Lemmon et al., 2018) to the model will allow for the calculation of refrigerant Transport Properties. And thus, allowing for calculation of heat transfer coefficients using the correlations available in the TIL Suite (2019). Additionally, to improve controls development a Functional Mock-Up Interface (FMI) should be created of Modelica model. The FMI standard sets forth a standardized method on how to exchange dynamic models between software. Software such as Simulink and LabView. This is powerful tool because the full dynamics of the model are captured within the FMU.

REFERENCES

AHRI-Standard-540-2015 (2015). Performance rating of positive displacement refrigerant compressors and compressor units. Air Conditioning and Refrigeration Institute Arlington, VA, USA.

Bitzer (2014). Refrigerant report 18. Technical Report A-501-18, Bitzer Kühlmaschinenbau GmbH, Sindelfingen, Germany.

Blochwitz, T., Junghanns, A., Köhler, J., and Krammer, M. (2019). Overview on FMI, SSP, DCP. 13th International Modelica Conference, Regensburg, Germany.

Bradshaw, C. (2014). Compressor performance measurements using hot-gas bypass load stands. Lecture presented at Short Course on Experimental Techniques to Measure Compressor Performance and Reliability in Purdue University, West Lafayette, IN.

Cai, J. and Braun, J. E. (2018). Assessments of variable-speed equipment for packaged rooftop units (rtus) in the united states. *Energy and Buildings*, 164:203 – 218.

Danfoss (2018a). Data sheet, Electric expansion valve, type ETS 12.5 – ETS 400. Retrieved from Danfoss website. **URL**: `https://assets.danfoss.com/documents/DOC285534162492/DOC285534162492.pdf`.

Danfoss (2018b). Heat exchanger design software. Danfoss hexact 5, version 5.4.4 [computer software].

Dassault Systèmes (2019). *What is Dymola?* Dassault Systèmes, Vélizy-Villacoublay, France.

EIA (2011). Emissions of greenhouse gases in the U.S. Technical report, U.S. Energy Information Administration. Retrieved May 3, 2019 **URL**: `https://www.eia.gov/environment/emissions/ghg_report/ghg_gwp.php`.

Emerson-Copeland (2020a). Emerson performance calculator. excel program [computer software]. Accessed on 01/28/2019.

Emerson-Copeland (2020b). Online product information, ZPV0962E-7E9. **URL**: `https://climate.emerson.com/en-us/tools-resources/online-product-information`.

Fritzson, P. (2014). *Principles of object-oriented modeling and simulation with Modelica 3.3*. Wiley.

Jain, N. and Alleyne, A. G. (2009). Comparison of SISO and MIMO control techniques for a diagonally dominant vapor compression system. In *2009 American Control Conference*, pages 1580–1585.

Kaiser, C., Sebastian, S., Tegethoff, W., and Köhler, J. (2018). Investigation of fuel reduction potential of a capacity controlled HVAC system for buses using virtual test drives. *Proceedings of The American Modelica Conference 2018, October 9-10, Somberg Conference Center, Cambridge MA, USA*, pages 7–16. **URL**: `https://ep.liu.se/ecp/article.asp?issue=154&article=001&volume=0#`.

Kang, H., Joo, Y., and Kim, Y. (2008). Effects of flash gas generation at the expansion device inlet on the dynamic characteristics of a refrigeration system. *International Journal of Refrigeration*, 31:396–403.

Kennedy, J. (2019). Personal communication on 04/18/2019, E-mail subject, Oklahoma State University: Braze Plate Heat Exchanger Concerns.

Kincheloe, M. C., Franke, J. P., Bach, C. K., and Bradshaw, C. R. (2021). Design of a psychrometric coil testing facility for commercial size heat exchanger coils. *International Journal of Refrigeration*, 121.

Klein, S. and Alvardo, F. (2020). *EES: Engineering equation solver, Academic Professional Version.*

Lemmon, E. W., , Bell, I. H., Huber, M. L., and McLinden, M. O. (2018). NIST Standard Reference Database 23: Reference Fluid Thermodynamic and Transport Properties-REFPROP, Version 10.0, National Institute of Standards and Technology.

Marcinichen, J. B., Holanda, T. N. d., and Melo, C. (2008). A dual SISO controller for a vapor compression refrigeration system. *International Refrigeration and Air Conditioning Conference*. Paper 922. **URL**: `https://docs.lib.purdue.edu/iracc/922/`.

MATLAB (2020). *Version 9.9.0 (R2020b)*. The MathWorks Inc., Natick, Massachusetts.

National Instruments (2009). *LabVIEW control design user manual.* National Instruments Corporation, Austin, TX.

Orosz, J., Bradshaw, C., Kemp, G., and Groll, E. (2016). Updated performance and operating characteristics of a novel rotating spool compressor. *International Compressor Engineering Conference*. Paper 2467. **URL**: `https://docs.lib.purdue.edu/icec/2467`.

Rahman, M., Sarkar, S. K., Das, S. K., and Miao, Y. (2017). A comparative study of LQR, LQG, and integral LQG controller for frequency control of interconnected smart grid. In *2017 3rd International Conference on Electrical Information and Communication Technology (EICT)*, pages 1–6.

Richey, J., Alhassan, M., Franco, V., and Alshammari, K. (2020). Senior Design Final Project Report: Hot Gas Bypass Chiller. Technical report, Oklahoma State University, Mechanical and Aerospace Engineering.

Schmidt, D., Singleton, J., and Bradshaw, C. (2019). Development of a light-commercial compressor load stand to measure compressor performance using low-GWP refrigerants. *International Journal of Refrigeration*, 100.

Singleton, J., Schmidt, D., and Bradshaw, C. R. (2020). Control and commissioning of a hot-gas bypass compressor load stand for testing light-commercial compressors on low-GWP refrigerants. *International Journal of Refrigeration*, 112:82 – 89.

Sporlan (2018). Electric hot gas bypass valves. Retrieved on September, 2019. **URL**: `https://sporlanonline.com/literature/100/ev/100-60%20Electric%20Hot%20Gas%20Bypass%20Valves.pdf`.

Tanveer, M. M. and Bradshaw, C. R. (2020). Quantitative and qualitative evaluation of various positive-displacement compressor modeling platforms. *International Journal of Refrigeration*, 119.

TIL Suite (2018). Software package for the simulation of thermal systems. TLK-Thermo GmbH, version 3.4 [computer software].

TIL Suite (2019). Software package for the simulation of thermal systems. TLK-Thermo GmbH, version 3.7 [computer software].

Trane (2003). Blessing or curse? Hot gas bypass. *Engineering Newsletter*, 32(2):1–4.

Winkler, J. (2009). *Development of a Component Based Simulation Tool for the Steady State and Transient Analysis of Vapor Compression Systems*. PhD thesis, University of Maryland, College Park, MD.

Yaqub, M., Zubair, S. M., and ur Rehman Khan, J. (2000). Performance evaluation of hot-gas by-pass capacity control schemes for refrigeration and air-conditioning systems. *Energy*, 25:543–561. **URL**: `http://www.sciencedirect.com/science/article/pii/S0360544200000049`.

Ziegler, J. G. and Nichols, N. B. (1985). Optimum settings for automatic controllers. *Journal of Dynamic Systems, Measurement, and Control*, 115(2B):220.

APPENDIX A

EES Steady State Modeling and Component Selection Code

"Inputs"

"Temperatures"
//T_sup=11.1[C]
//T_sub=8.3[C]
//T_con=32[C]
//T_evap=-3[C]

"Cooling Water Temps"

//Tc_in=converttemp(F,C,70)
//Tc_out=converttemp(F,C,80)

"Compressor Speed"
//n=120   "Hz"

"Modelica Array Table Comparison"
"Compressor suction"
P_m[1]=730.2
h_m[1]=430.5

"Condenser inlet"
P_m[2]=2068
h_m[2]=528.3

"Subcooler inlet"
P_m[3]=2068
h_m[3]=251.6

"Expansion Valve inlet"
P_m[4]=2068
h_m[4]=239.4

"Evaporator inlet"
P_m[5]=730.2
h_m[5]=239.4

"Evaporator outlet"
P_m[6]=730.2
h_m[6]=430.5

"Compressor"

T[1]=T_evap+T_sup
P[1]=**pressure**(R$, *T*=T_evap, *x*=1)
h[1]=**enthalpy**(R$, *T*=T[1], *P*=P[1])
s[1]=**entropy**(R$, *T*=T[1], *P*=P[1])
rho[1]=**density**(R$, *T*=T[1], *P*=P[1])

P[2]=**pressure**(R$,*T*=T_con, *x*=0)
h_s[2]=**enthalpy**(R$, *P*=P[2], *s*=s[1])
T_s[2]=**temperature**(R$, *P*=P[2], *s*=s[1])+28[C]
h[2]=(h_s[2]-h[1]+ETA_comp*h[1])/ETA_comp_n
T[2]=**temperature**(R$, *P*=P[2], *h*=h[2])

s[2]=**entropy**(R$, *T*=T[2], *P*=P[2])
rho[2]=**density**(R$, *T*=T[2], *P*=P[2])

"Bypass Valve"

h[7]=h[2]

48

P[7]=P[2]
T[7]=**temperature**(R$, *P*=P[7], *h*=h[7])
s[7]=**entropy**(R$, *P*=P[7], *h*=h[7])
rho[7]=**density**(R$, *P*=P[7], *h*=h[7])

h[6]=h[2]
P[6]=P[1]
T[6]=**temperature**(R$, *P*=P[6], *h*=h[6])
s[6]=**entropy**(R$, *P*=P[6], *h*=h[6])
rho[6]=**density**(R$, *P*=P[6], *h*=h[6])

"Condenser"

T[3]=T_con
P[3]=**pressure**(R$, *T*=T_con, *x*=0)
h[3]=**enthalpy**(R$,*T*=T[3], *x*=0)
s[3]=**entropy**(R$, *T*=T[3], *x*=0)
rho[3]=**density**(R$, *T*=T[3],*x*=0)

"Subcooler"

T[4]=T_con-T_sub
P[4]=P[3]
h[4]=**enthalpy**(R$,*T*=T[4], *P*=P[4])
s[4]=**entropy**(R$, *P*=P[4], *h*=h[4])
rho[4]=**density**(R$, *P*=P[4],*h*=h[4])

"Liquid Expansion Valve"

h[5]=h[4]
P[5]=P[1]
T[5]=**temperature**(R$, *P*=P[5], *h*=h[5])
s[5]=**entropy**(R$, *P*=P[5], *h*=h[5])
rho[5]=**density**(R$, *P*=P[5], *h*=h[5])

"system"

$ifnot Parametric then

R$='R410A'
$endif

"Drive Output Power"
w_dot_isn_20 = mdot_tot_20*(h_s[2]-h[1])***convert**(kW,W)
w_dot_act_20 = 2.77E+01 - 6.07E+01*T_evap + 7.63E+01*T_con - 2.27E+00*T_evap^2 + 2.33E+00*T_evap*T_con - 1.09E+00*T_con^2 - 1.62E-02*T_evap^3 + 4.37E-02*T_evap^2*T_con - 2.26E-02*T_evap*T_con^2 + 1.45E-02*T_con^3

w_dot_isn_120 = mdot_tot_120*(h_s[2]-h[1])***convert**(kW,W)
w_dot_act_120 = 7.15E+03 - 8.01E+01*T_evap + 2.04E+02*T_con - 3.18E+00*T_evap^2 + 4.38E+00*T_evap*T_con + 1.93E-01*T_con^2 - 1.62E-02*T_evap^3 + 4.37E-02*T_evap^2*T_con - 2.26E-02*T_evap*T_con^2 + 1.45E-02*T_con^3

"Efficiencies"
ETA_comp_20= w_dot_isn_20/w_dot_act_20
ETA_comp_120 = w_dot_isn_120/w_dot_act_120

ETA_comp=(1.05546964E+01+3.44817319E+00*T_con-6.24365132E-02*T_con^2+3.56140115E-04*T_con^3-2.85392910E+00*T_evap-6.36895272E-02*T_evap^2-3.97191250E-04*T_evap^3+1.10087824E-01*T_con*T_evap+9.38065216E-04*T_con*T_evap^2-8.87149443E-04*T_con^2*T_evap)/100

"Reference Data"

"Mass Flow Rate"
mdot_tot_120=(1.18E+03+7.41E-01*T_con-1.13E-02*T_con^2+0.00E+00*T_con^3+3.94E+01*T_evap+5.01E-01*T_evap^2+
2.17E-03*T_evap^3+2.15E-02*T_con*T_evap+0.00E+00*T_con*T_evap^2-1.54E-04*T_con^2*T_evap)***convert**(kg/hr,kg/s)

mdot_tot_20=(1.91E+02-1.04E-01*T_con-1.88E-03*T_con^2+0.00E+00*T_con^3+6.04E+00*T_evap+1.09E-01*T_evap^2+
2.17E-03*T_evap^3+3.59E-03*T_con*T_evap+0.00E+00*T_con*T_evap^2+-1.54E-04*T_con^2*T_evap)***convert**(kg/hr,kg/s)

"Variable Speed Interpolation"

(mdot_tot_n-mdot_tot_20)/(mdot_tot_120-mdot_tot_20)=(n-20)/(120-20)

(ETA_comp_n-ETA_comp_20)/(ETA_comp_120-ETA_comp_20)=(n-20)/(120-20)

m_dot_tot = mdot_tot_n
m_dot_c = mdot_c

"Energy Balance/Bypass Flow Variation"
//epsilon=0   "percent of bypass flowrate"

m_dot_bypass=epsilon*mdot_c*((h[1]-h[5])/(h[6]-h[1]))

m_dot_bypass=mdot_tot_n-mdot_c

Q_dot_bypass=m_dot_bypass*(h[6]-h[1])

"Cooling Capacity"
Q_dot_cool=mdot_c*(h[1]-h[4])

"Heat Rejection"
Q_dot_hot=mdot_c*(h[2]-h[3])

"Q_dot Subcooler"
Q_dot_sc=mdot_c*(h[3]-h[4])

Din_w=1.05[in]***convert**(in,m)

cp_w_in=**cp**(*Water*,*T*=Tc_in,*P*=P[4])
cp_w_out=**cp**(*Water*,*T*=Tc_out,*P*=P[4])

cp_w=(cp_w_in+cp_w_out)/2

mdot_w=Q_dot_hot/(cp_w*(Tc_out-Tc_in))

rho_w_in=**density**(*Water*,*T*=Tc_in,*P*=P[4])
rho_w_out=**density**(*Water*,*T*=Tc_out,*P*=P[4])

rho_w=(rho_w_in+rho_w_out)/2

Vavg_w=mdot_w/(rho_w*(pi/4)*(Din_w)^2)
V_dot_w=mdot_w/rho_w***convert**(m^3/s,gpm)

m_dot_w_cond = mdot_w

"rule of thumb"

"refrigerant"
m_dot_r=mdot_tot_n
cp_r_out=**cp**(R$,*T*=T[3],*P*=P[3])
cp_r_in=**cp**(R$,*T*=T[2],*P*=P[2])
cp_r=(cp_r_in+cp_r_out)/2
"water"
V_dot=33[gpm]***convert**(gpm,m^3/s)   "3 gpm*16.4 tons"
m_dot_w=rho_w*V_dot
m_dot_w*cp_w*(Tc_out_w-Tc_in)=mdot_c*(h[2]-h[3])

m_dot_w_sc=Q_dot_sc/(cp_w*(Tc_out-Tc_in))

"Suction/discharge line interpolations"
"suction"
T_40=40[F]
T_20=20[F]
T_ss= **converttemp**(C,F,T_evap)
(T_ss-T_20)/(T_40-T_20)=(X_ton_suc-17.14)/(24.28-17.14)   "capacity for 1
5/8"
Q_s=X_ton_suc
Q_suc=Q_s***convert**(ton,kW)
h_con=**enthalpy**('R410A', *T*=40[C], *x*=0)   "105F from table 8 ashrae 2018"
h_evap=**enthalpy**('R410A', *T*=T_evap, *x*=1)
m_dot_suc=Q_suc/(h_evap-h_con)

"discharge"
(T_ss-T_20)/(T_40-T_20)=(X_ton_dis-22.37)/(22.88-22.37)   "capacity for 1
3/8"
Q_d=X_ton_dis
Q_dis=Q_d***convert**(ton,kW)
h_c=**enthalpy**('R410A', *T*=40[C], *x*=0)
h_e=**enthalpy**('R410A', *T*=T_evap, *x*=1)
m_dot_dis=Q_dis/(h_e-h_c)

"Liquid Line"
ID=.875[in]
A_in=(pi/4)*ID^2
A_in_m2=A_in***convert**(in^2,m^2)
V_dot_ll=mdot_c/rho[4]
v_ll=V_dot_ll/A_in_m2***convert**(m/s,ft/min)

"Acumulator Sizing"
"mass_100% - mass_0% capacity"

V_evap = 6.049E-3 [m^3]
rho_evap_100 = rho[5]
rho_evap_0 = rho[1]
DELTA_m_evap=V_evap*(rho_evap_100 - rho_evap_0)

"Receiver Sizing"
"mass_100% - mass_0% capacity"

V_cond = 3.96E-3 [m^3]
rho_cond_100 = rho[3]
rho_cond_0 = rho[2]
DELTA_m_cond=V_evap*(rho_cond_100 - rho_cond_0)

"Total Volume calculation"

V_pipe = 0.00246 [m^3]
V_com = 9.636e-5 [m^3]
V_sub = 0.000315 [m^3]
"mass = mass_pipe(liquid) + mass_pipe(gas_l) + mass_pipe(gas_h) + mass_compressor + mass_cond + mass_evap + mass_subcooler"
m_tot = rho[4]*(.33*V_pipe) + rho[2]*(.33*V_pipe)+ rho[5]*(.33*V_pipe) + ((rho[1]+rho[2])/2)*V_com + rho_cond_100*V_cond + rho_evap_100*V_evap + rho[4]*V_sub

"Parker Hannifin Corporation Catalog C-1, Accumlators and Receivers pg. 4"
"Systems with TXV or changing orifice size, the accumlator should be about 50% of system charge"
m_acc = .5*m_tot

APPENDIX B

MATLAB System ID Code

```matlab
1  %% System Identification - Khurram Makhani
2
3  %% Read File
4  % NX7 Matrix from excel with all values
5  matrix = readmatrix('Random');
6  % Time [sec] start at 60 sec into SIMULATION
7  time = matrix(650:13250,1);
8  % EXV effective flow area [m^2]
9  EXV_efa = matrix(650:13250,2);
10 % HGBV effective flow area [m^2]
11 HGBV_efa = matrix(650:13250,3);
12 % Delta Super Heat [K]
13 SH = matrix(650:13250,4);
14 % Suction Pressure [bar]
15 P_suc = matrix(650:13250,5)/1e5;
16 % Mass Flow Pumped Refrigerant [kg/s]
17 m_dot = matrix(650:13250,6);
18 % Frequency of compressor
19 n = matrix(650:13250,7);
20 % T Con
21 T_con = matrix(650:13250,8);
22 %% Normalizing Data
23 % Outputs
24
25 % Super Heat
26 % Set Point = 11 [K]
27 % Max SH = 21 [K], Min SH = 1 [K]
28 % Super heat normalized from -1 to 1
29 SH_n = (SH-11)/10;
30
31 % Suction Pressure
32 % Set Point = 725 [kPa]
33 % Max P_suc = 775 [kPa], Min P_suc = 675 [kPa]
34 % Suction Pressure normalized from -1 to 1
35 P_suc_n = (P_suc-7.25)/.50;
36
37 % Suction Saturated Temp
```

```matlab
38 % Set Point = −2.5 [C]
39 % Max T_sat = −.5 [C], Min T_sat = −4.5 [C]
40 % Suction Saturated Temperature normalized from −1 to 1
41 % T_sat_n = (T_sat+2.5)/2;
42
43 % Inputs
44
45 % HGBV EFA
46 % Set Point = 1.9e−5 [m^2]
47 % Max HGBV_efa = 2.1e−5 [m^2], Min HGBV_efa = 1.7e−5 [m^2]
48 % HGBV Position normalized from −1 to 1
49 HGBV_efa_n = (HGBV_efa−1.9e−5)/.2e−5;
50
51 % EXV EFA
52 % Set Point = .18e−5 [m^2]
53 % Max EXV_efa = .20e−5 [m^2], Min EXV_efa = .16e−5 [m^2]
54 % EXV Position normalized from −1 to 1
55 EXV_efa_n = (EXV_efa−.18e−5)/.02e−5;
56
57 % m_dot
58 % Set Point = .012 [kg/s]
59 % Max m_dot = .013 [kg/s], Min m_dot = .011 [kg/s]
60 % EXV Position normalized from −1 to 1
61 m_dot_n = (m_dot−.012)/.001;
62
63 % n
64 % Set Point = 120 hz
65 % Max n = 125 hz, Min n = 115 hz
66 % Frequency normalized from −1 to 1
67 n_n = (n−120)/5;
68
69 % T_con
70 % Set Point = 295 K
71 % Max T_con = 300 K, Min T_con = 290 K
72 % T_con normalized from −1 to 1
73 T_con_n = (T_con−295)/5;
74 %% System Identification
75 steam = iddata([SH_n,P_suc_n],[EXV_efa_n,HGBV_efa_n,n_n],1);
76 steam.InputName = {'EXV_efa_n';'HGBV_efa_n';'Compressor
       Speed_n'};
77 steam.OutputName = {'Superheat_n';'Suction Pressure_n'};
78
79
80
81 % plot(steam(:,:,:))
```

```matlab
82  % hold on
83  % %impluse response
84  % % Note impulseest(data, N), N=[] to let Matlab find order
        of FIR Model
85   mi = impulseest(steam,[]);
86  % figure(2)
87  % clf, step(mi)
88  % hold on
89  % figure(3)
90  % %Response with Confidence Region
91  % showConfidence(impulseplot(mi),3)
92
93  %MIMO: Estimate State Space Model using time domain "ssest"
94
95   [mp, X0] = ssest(steam(1:6300),2,'DisturbanceModel','none','
        Ts',1)
96   figure(1)
97
98  %h = stepplot(mi,'b',mp,'r',2); % Blue for direct estimate,
        red for mp
99  % showConfidence(h)
100 % Compare with validation data
101 %figure(2)
102 compare(steam(1:12601),mp)
103 %save('matrix.mat','steam');
104 % Spectral analysis of data
105 %msp = spa(steam);
106 %clf, bode(msp,'b',mp,'r')
```

APPENDIX C

MATLAB LQR Controller Code

```
1  A=mp.A;
2  B=mp.B;
3  C=mp.C;
4  D=mp.D;
5  n = length(A); % dimension of the system
6  Bu = B(:,1:2); % control input
7  Bd = B(:,3); % disturbance input
8  m = 2; % dimension of the control
9  %% controller I: LQR with disturbance input
10 Qo = eye(2); % output dimension is 2
11 Q = C'*Qo*C; % take it back to the full state
12 R = eye(m); % Q and R can be adjusted
13 [F,P,~] = dlqr(A,Bu,Q,R);
14 S = inv(A*inv(P-Q)-inv(P))*Bd;
15 G = F*inv(A-inv(P)*(P-Q))*Bd;
16 % implement control as u = -F*x - G*d where d is the
       disturbance, x is full
17 % state (easiest to implement when x is 2-dimensional, in
       this case x =
18 % inv(C)*[super heat;suc pressure];
```

APPENDIX D

Modelica MIMO Code

```
1  within ;
2  block MIMO_HGBC "MIMO Block Utilizing LQR Control"
3    extends Modelica.Blocks.Interfaces.MIMO(nin=3,nout=2);
4
5    //parameter Real K[:, :]=[-0.5857, -0.1210; -1.5896,
        0.0566; 0.2252, 0.0300]
6      //"Gain matrix which is multiplied with the input";
7    parameter Real C_inv[:, :]=[0, 0; 0, 0]
8      "C inverse matrix which is multiplied by inputs to
          achieve states";
9    parameter Real F[:, :]=[0, 0; 0, 0]
10     "F Matrix";
11   parameter Real G[:, :]=[0, 0; 0, 0]
12     "G Matrix";
13   Real SH = u[1]
14     "Superheat [K]";
15   Real P_suc = u[2]/1e5
16     "Suction Pressure [Bar]";
17   Real n = u[3]
18     "Compressor Speed [Hz]";
19   Real SH_n=(SH-11)/10
20     "SH normalized [-1 to 1]";
21   Real P_suc_n=(P_suc-7.25)/0.5
22     "P_suc normalized [-1 to 1]";
23   Real u_n[:,:]=[SH_n; P_suc_n]
24     "normalized column vector";
25   Real x[:,:]=C_inv*u_n
26     "State of System";
27   Real d=(n-120)/5
28     "Disturbance nomalized";
29   Real u_out[:,:] = (-F*x)-(G*d)
30     "Output from LQR";
31
32 equation
33
34   y[1] = max(0.1e-5,u_out[1,1]*(0.02e-5)+0.18e-5);
35   y[2] = max(1e-5,u_out[2,1]*(0.2e-5)+1.9e-5);
```

```modelica
36
37  annotation (Icon(coordinateSystem(preserveAspectRatio=
        false)), Diagram(
38          coordinateSystem(preserveAspectRatio=false)),
39          Documentation(info="<html>
40          <p>This block provides a LQR Controller for MIMO
              Control.</p>
41          </html>
42          "));
43  end MIMO_HGBC;
```
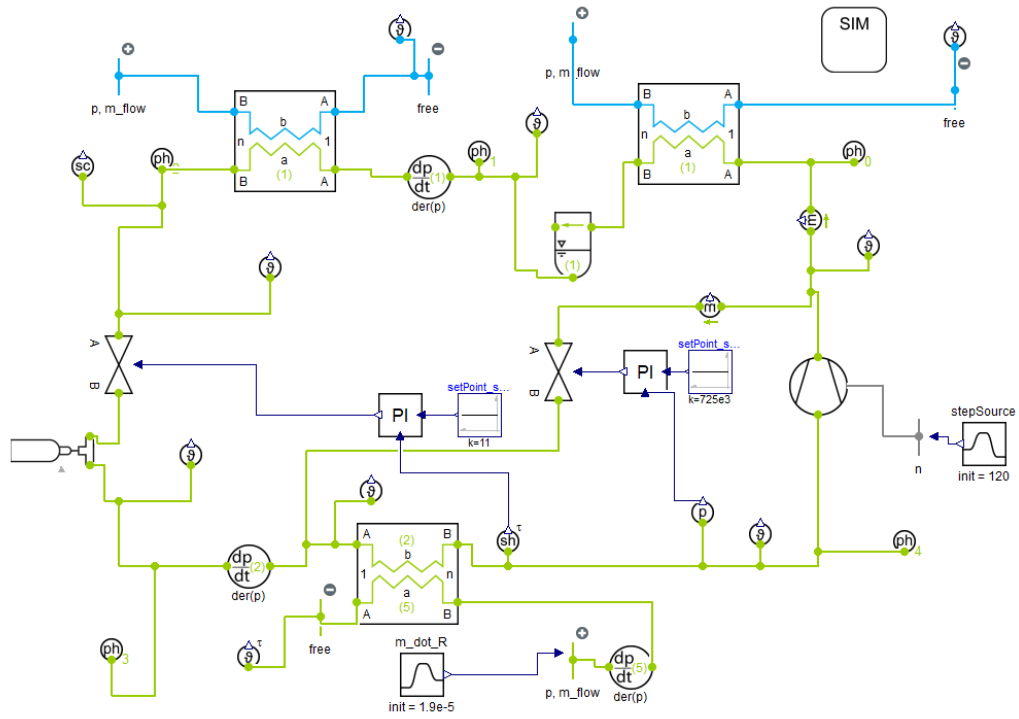
APPENDIX E

Modelica Diagram Window

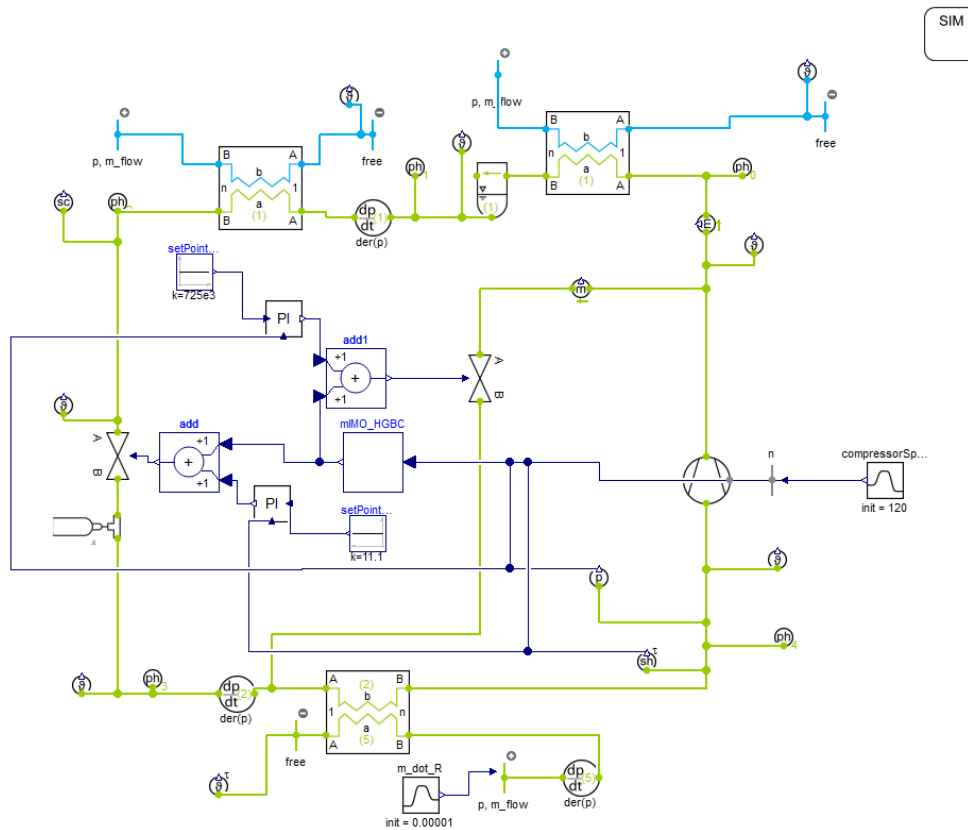Figure E.1: SISO PI Controls - Dymola Diagram Window

Figure E.2: MIMO LQR Controller - Dymola Diagram Window

5.1 RefProp for Property Calculations with TIL Library Using Dymola

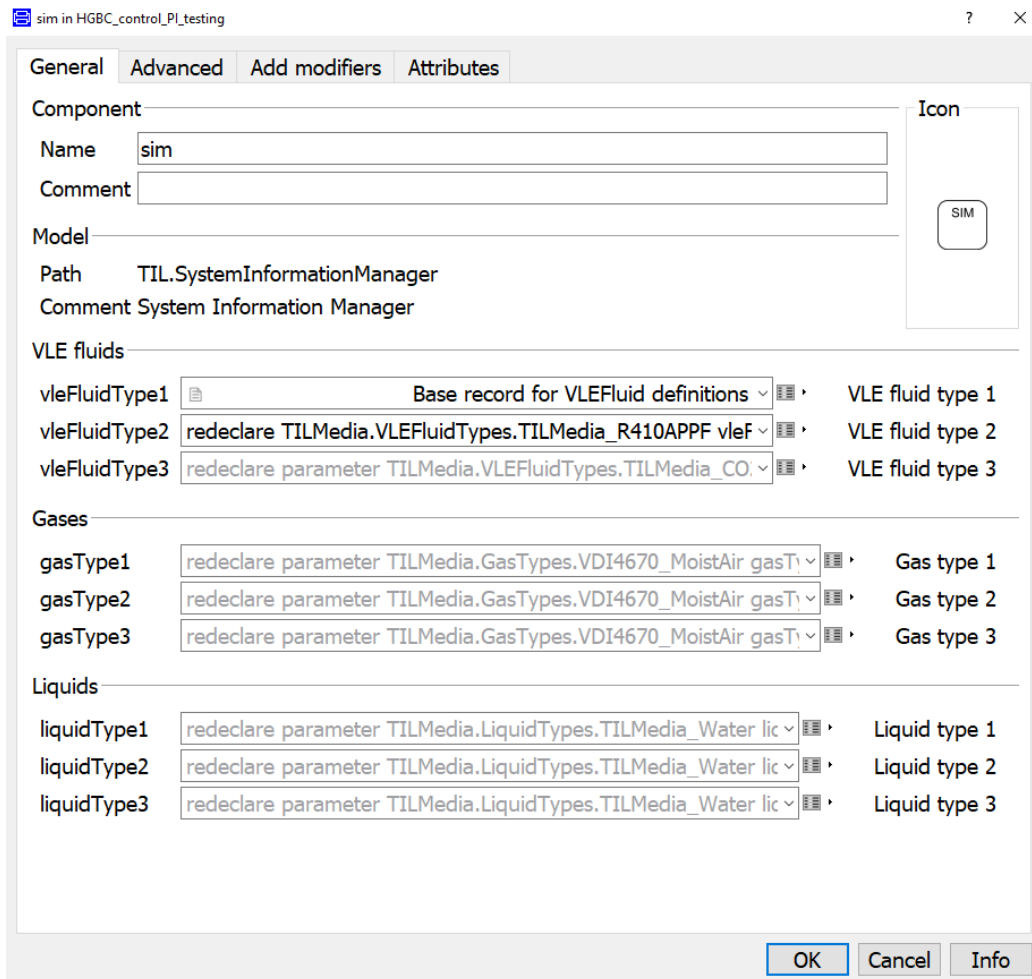First, select the System Information Manager (SIM) tab to edit fluid definitions.

Figure E.3: SIM Tab

Modify the *vleFluidType1* definition to "Base record for VLEFluid definitions". Then select the edit tab to the right of the drop down menu for *vleFluidType1* definition. After selecting the edit tab, a new window will appear for re-declaration of *vleFluidType1*.

Select the edit tab to the right of *vleFluidNames*. After selecting the edit tab, a new window will appear for editing the *vleFluidType1* array.

If one fluid is to be selected leave the Row length equal to 1. Then select the drop down menu to select the vleFluidType.
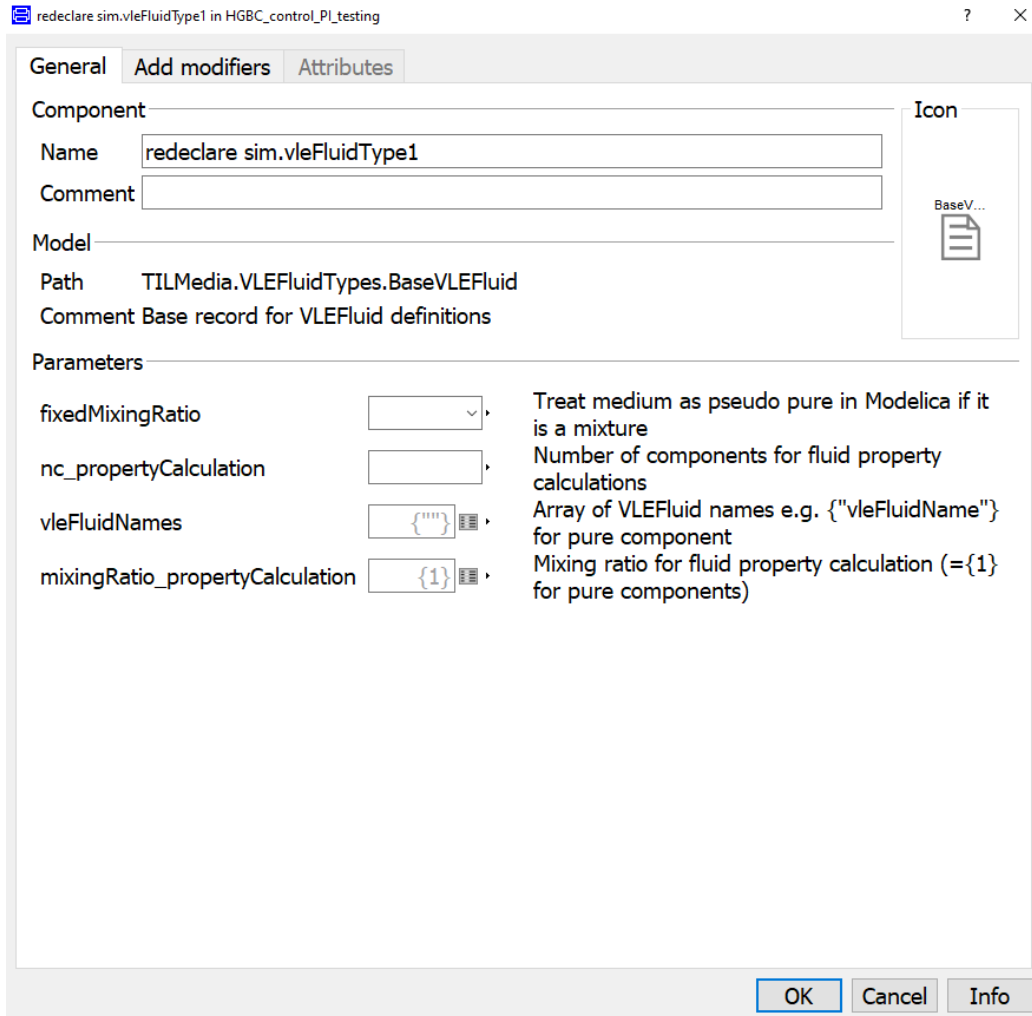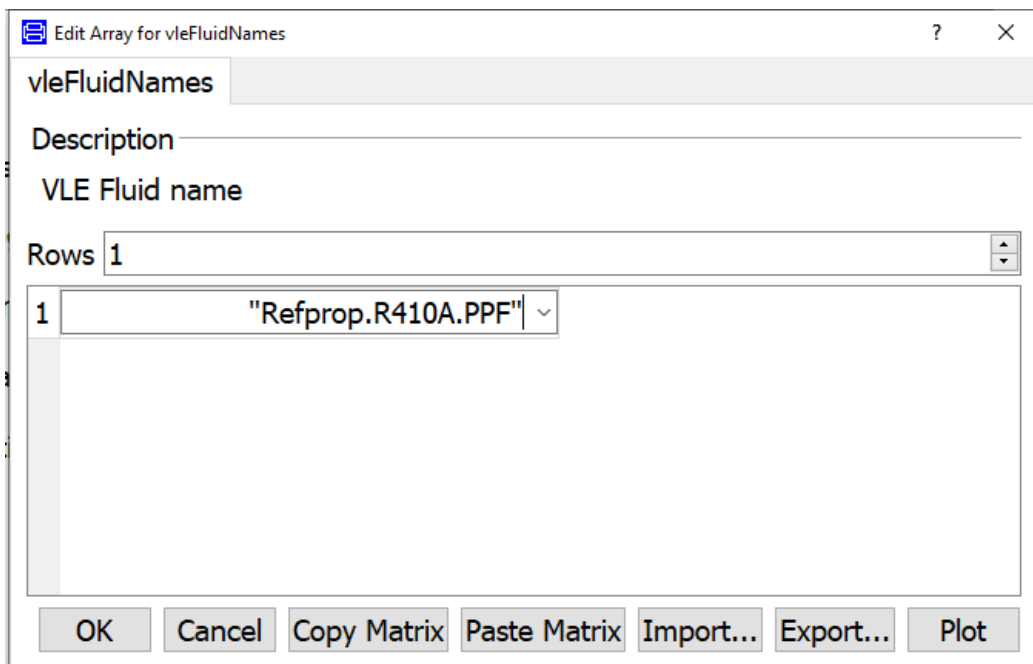
Figure E.4: Redeclare Tab

Figure E.5: Edit Array Tab
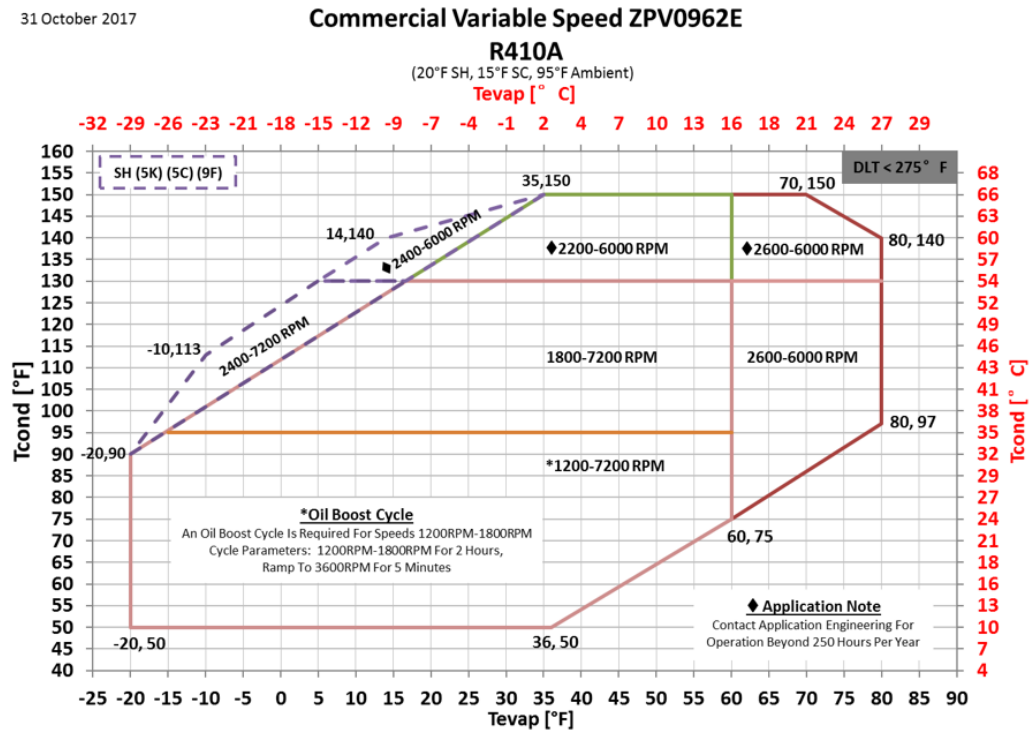
APPENDIX F

Compressor Operating Envelope

Figure F.1: Compressor Performance Envelope - (Emerson-Copeland, 2020b)

VITA

Khurram K. Makhani

Candidate for the Degree of

Master of Science

Thesis: Design, Simulation, and Construction of a Hot-Gas Bypass Chiller for a Commercial Scale Psychrometric Coil Testing Facility

Major Field: Mechanical Engineering

Biographical:

Education:
Received a Bachelors of Science in Mechanical Engineering at Oklahoma State University in May 2018.
Completed the requirements for the degree of Master of Science with a major in Mechanical Engineering at Oklahoma State University in November 2020.